Dinarès-Turell, J., Pujalte, V., Stoykova, K. y Elorza, J. 2013. Detailed correlation and astronomical forcing within the Upper Maastrichtian succession in the Basque Basin. *Boletín Geológico y Minero,* 124 (2): 253-282
ISSN: 0366-0176

Detailed correlation and astronomical forcing within the Upper Maastrichtian succession in the Basque Basin

J. Dinarès-Turell[(1)], V. Pujalte[(2)], K. Stoykova[(3)] y J. Elorza[(4)]

(1) Istituto Nazionale di Geofisica e Vulcanologia, Via di Vigna Murata 605, I-00143 Rome, Italy
(2) Department of Stratigraphy and Paleontology, Fac. Science and Technology, University of the Basque Country UPV/EHU, PO Box 644, E-48080 Bilbao, Spain
(3) Department of Paleontology and Stratigraphy, Geological Institute, Bulgarian Academy of Science, BG-1113 Sofia, Bulgaria
(4) Department of Mineralogy and Petrology, Fac. Science and Technology, University of the Basque Country UPV/EHU, PO Box 644, E-48080 Bilbao, Spain

ABSTRACT

We have undertaken a comprehensive, integrated, cyclo-magnetostratigraphic analysis and study of the calcareous nannofossils of the Upper Maastrichtian hemipelagic succession in three sections of the Basque Basin (Zumaia, Sopelana and Hendaia). The sections were correlated at bed-by-bed scale through careful analysis of the lithological stacking pattern and significant sedimentary features. For spectral analysis we used an available high-resolution carbonate proxy record spanning 64 m of section below the K/Pg (Cretaceous/Palaeogene) boundary at Zumaia containing 72 precession-related limestone-marl couplets. The continuous wavelet spectrum helped to determine and visualize the orbital forcing at both the short (~100-ky) and long (405-ky) eccentricity band. We applied bandpass Gaussian filters to the carbonate record to extract the relevant periodicities and provide a cycle-numbering scheme starting at the K/Pg boundary. The full hierarchy of precession cycles and eccentricity-related bundles is then extended toward the base of the section in question, which contains a total of 33 short eccentricity-related bundles, thus spanning more than 3 Ma. The chron C31r/C31n boundary (estimated to occur at ~3.08 Ma below the K/Pg boundary) in the lower part of the succession was determined unambiguously in all three sections studied although the C30n/C29r reversal could not be determined due to a pervasive reverse magnetization acting on the purplish lithologies in the upper part of the succession. Relevant calcareous plankton bioevents could be accurately placed on the cyclo-magnetostratigraphic template. The cyclostratigraphic framework also allowed us to estimate the duration of previously defined sea-level-related 3rd-order depositional sequences in the basin, which appear to be strongly paced by the long-term 1.2 My obliquity amplitude modulating cycle. This is an outstanding feature in the Maastrichtian greenhouse period, during which continental ice sheets are expected to be either ephemeral or non-existent. This is a matter that deserves further attention.

Key words: calcareous nannofossils, cyclostratigraphy, depositional sequences, Milankovitch, magnetostratigraphy

Correlación detallada y control orbital de la sucesión del Maastrichtiense Superior de la Cuenca Vasca

RESUMEN

Se presenta un estudio exhaustivo ciclo-magnetostratigráfico y de nanofósiles calcáreos de tres secciones de la sucesión hemipelágica del Maastrichtiense Superior de la Cuenca Vasca (Zumaia, Sopelana y Hendaia). La correlación entre secciones se realiza capa a capa mediante un análisis minucioso del patrón del apilamiento litológico y detalles sedimentarios. Para el análisis espectral se utiliza un registro de carbonato de alta resolución de un intervalo de 64 m debajo del límite K/Pg (Cretácico/Paleógeno), disponible en Zumaia, que contine 72 pares marga-caliza relacionados con el ciclo de precesión. El espectro continuo de ondas pequeñas ayuda a determinar y visualizar el control orbital en las bandas de la excentricidad corta (~100-ka) y larga (405-ka). Se han usado filtros gausianos pasabanda sobre el registro de carbonato para extraer las periodicidades relevantes y se aporta un esquema de numeración de ciclos que se inicia en el límite K/Pg. A continuación, la jerarquía

completa de ciclos de precesión y paquetes de la excentricidad se ha extendido hacia la base de la sucesión estudiada, que contiene un total de 33 paquetes relacionados con la excentricidad corta y en consecuencia una duración superior a los 3 Ma. El límite de cron C31r/C31n (posición estimada a ~3.08 Ma debajo del K/Pg) se ha determinado de forma inequívoca en la parte inferior de la sucesión en las tres secciones estudiadas, pero no ha sido posible determinar el límite de cron C30n/C29r debido a una remagnetización inversa generalizada en las litologías rojizas de la parte superior de la sucesión. Los bioeventos relevantes del plankton calcáreo pueden posicionarse con precisión en el modelo ciclo-magnetostratigráfico. Además, la plantilla ciclostratigráfica permite estimar la duración de las secuencias deposicionales de 3er-orden relacionadas con variaciones del nivel del mar que han sido definidas con anterioridad en la cuenca, y que parecen gobernadas por el ciclo de 1.2 Ma de la oblicuidad de modulación de la amplitud. Esto representa un hecho destacado para el periodo invernadero del Maastrichtiense en el que se cree que los casquetes glaciares continentales fueron efímeros o no existentes, y es un aspecto que necesita ser estudiado con más profundidad.

Palabras clave: ciclostratigrafía, Milankovitch, magnetostratigrafía, nanofósiles calcareos, secuencias deposicionales

VERSION ABREVIADA EN CASTELLANO

Introducción y metodología

La correlación astronómica o "tuning" de secuencias que presentan ciclos litológicos con soluciones orbitales proporcionadas por los astrónomos ha conducido a una resolución y precisión sin precedentes en el registro geológico a lo largo de gran parte del Cenozoico. Para el Paleógeno, la correlación astronómica resulta complicada a pesar de la existencia de soluciones numéricas modernas para el Sistema Solar (Varadi et al.*, 2003; Laskar* et al.*, 2004), debido a imprecisiones y limitaciones inherentes al comportamiento caótico del Sistema Solar y a un pobre control con edades radiométricas. Las sucesiones hemipelágicas paleocenas de la Cuenca Vasca han contribuido a un vivo debate sobre la extensión de la calibración astronómica para esta época que aún no ha sido resuelta satisfactoriamente (Dinarès-Turell* et al.*, 2003, 2007, 2010, 2012; Westerhold* et al.*, 2008, 2011; Kuiper* et al.*, 2008; Hilgen* et al.*, 2010). Los primeros intentos de correlación astronómica para el Cretácico considerando el límite K/Pg y algunos crones magnéticos se basaron en duraciones relativas (e.g. Herbert* et al. *1995, Herbert, 1999). Solo recientemente el Maastrichtiense ha sido calibrado astronómicamente usando soluciones modernas (Husson* et al.*, 2011; Thibault* et al.*, 2012). En este trabajo presentamos el primer estudio detallado integrado ciclo- magnetostratigráfico y de nanofósiles calcáreos para la sucesión del Maastrichtiense Superior de la Cuenca Vasca.*

El Maastrichtiense de la Cuenca Vasca está expuesto en diferentes afloramientos a lo largo de la costa que han sido clásicamente estudiados principalmente por su contenido biostratigráfico (Fig. 1). El origen orbital de las alternancias marga-caliza también ha sido estudiado con anterioridad (Mount and Ward, 1986; Ten Kate and Sprenger, 1993). Recientemente un estudio integrado de plankton calcáreo y magnetostratigrafía ha sido publicado para la sección de Zumaia aunque no presenta un log litológico detallado ni se ha abordado la ciclicidad (Pérez-Rodríguez et al.*, 2012). La mayor parte del Maastrichtiense de la Cuenca Vasca consiste en una alternancia de margas y carbonatos hemipelágicos, y en algunas secciones, turbiditas finas/medias (cm a dm de espesor). Atendiendo la proporción variable de esas litologías, se hizo una subdivisión litoestratigráfica formal en miembros (Miembros I a V de Ward, 1988; Ward y Kennedy, 1993) y una informal más detallada en unidades (unidades 2 a 12 de Wiedmann, 1988) (Fig. 2). Las variaciones litológicas de escala mayor a lo largo de la sucesión también han sido interpretadas por autores más recientes en términos de estratigrafía secuencial (Pujalte* et al.*, 1995; Baceta* et al.*, 2004), que han reconocido 3 secuencias deposicionales de 3er orden. En este trabajo las tres secuencias deposicionales se han renombrado de más antigua a más moderna como UMa-1, UMa-2 and Ma-Da respectivamente (Fig. 2).*

Este trabajo se centra en el intervalo que comprende las unidades 6–12, que engloba el Maastrichtiense Superior, a lo largo de tres secciones (Zumaia, Sopelana I y Hendaia) (Fig. 1, Fig. 3). Un análisis cuidadoso en las secciones ha posibilitado una correlación capa a capa que ha permitido establecer una cronología astronómica para el intervalo estudiado. Un registro de carbonato de alta resolución para las unidades 10-12 en Zumaia (Ten Kate and Sprenger, 1993) se ha utilizado para nuevos análisis espectrales y determinar las periodicidades, las fases y la correlación astronómica correspondientes. La arquitectura deposicional y el contaje de los pares marga-caliza atribuidos a la precesión astronómica (~21 ka) y los ciclos de excentricidad (~100 ka) (grupos de 4–6 pares marga-caliza) se han establecido para todo el interval estudiado. El anclaje con la solución astronómica se ha basado en la presencia de los ciclos de excentricidad de 405 ka y la edad del límite K/Pg. Asimismo se ha realizado un estudio magnetostratigráfico para intervalos seleccionados en Zumaia y Sopelana I y hemos realizado un estudio de alta resolución de nanofósiles calcáreos en Sopelana I que no disponía de estos datos.

Para el estudio magnetostratigráfico se han seleccionado las partes relevantes en las diversas secciones estudiadas (Fig. 2). El muestreo se ha realizado a una resolución mínima de una muestra por par litológico e incluye la inversión del cron C30n/29r alrededor del límite de las unidades 11/12 en las secciones de Zumaia (16 capas), Sopelana I (43 capas) y Hendaia (9 capas), y la inversión C31r/C31n en la unidad 6 en Zumaia (33 capas), Sopelana I (13 capas) y Hendaia (10 capas). Para el estudio de los nanofósiles de la sección de Sopelana I se han analizado 76 muestras desde el límite K/Pg hasta la parte inferior de la Unidad 6 (~67 m de espesor) y se ha adoptado el esquema de biozonas UC de Burnett (1998) (Fig. 4).

Resultados y discusión

A continuación se describen los resultados integrados para las secciones principales de Zumaia y Sopelana I en orden estratigráfico inverso siguiendo las unidades de Wiedmann (1988) y separadamente al final los resultados de la sección de Hendaia.

Las unidades 12–10 afloran en condiciones excepcionales en los acantilados de Punta Aitzgorri en Zumaia (Fig. 5). Se reconocen un total de 72 ciclos con un espesor aproximado de 0.9 m en el intervalo considerado. Un estudio previo de alta resolución sobre el registro de carbonato cálcico demostró que efectivamente los pares litológicos en el Maastrichtiense representan ciclos astronómicos de precisión de ~21-ka de duración. El registro de carbonato de Ten Kate and Sprenger (1993) se ha usado para extraer las periodicidades de los ciclos de excentricidad corta (~100-ka) y larga (~405-ka) a través del análisis espectral. En el diagrama de Fourier standard se reconocen tres periodicidades (Fig. 6). Una banda con periodos de 0.7-0.95 m está asociada al par litólogico relacionado con la precesión. Un periodo a 4.1 m se relaciona con la excentricidad corta de 100-ka mientras que el periodo a 17 m se puede asociar a la excentricidad larga de 405-ka. La Figura 7a muestra los ciclos de precesión (ciclos P_k1 to P_k72) y la distribución de los ciclos de excentricidad corta y larga extraídos a partir de filtros gaussianos correspondientes. Los ciclos de 405-ka se han nombrado $Ma_{405}1$, $Ma_{405}2$ y $Ma_{405}3$ mientras que los 17 ciclos de excentricidad de 100-ka deducidos a lo largo de las unidades 10–12 se han nombrado E1-E17. El estudio magnetostratigráfico (Fig. 8) realizado en la Unidad 11 demuestra que las llitologías rojizas de este intervalo presentan una remagnetización compleja por lo que no es posible establecer la posición de la inversión de crones C20n/C29r.

Los ciclos P_K1 a P_K72 también pueden distinguirse en la sección de Sopelana I tras resolver algunas fallas (Fig. 9). Los resultados magnetostratigráficos en la parte superior de la sección a lo largo de las unidades 12–10 indican que también existe una remagnetización generalizada (Fig. 10) por lo que no ha sido posible reproducir los resultados de estudios anteriores (Mary et al.*, 1991; Moreau* et al. *1994). El estudio de nanofósiles de la sección de Sopelana indica que estos son abundantes y representados por asociaciones muy diversificadas con una preservación de buena a muy buena (Plate I). Los bioeventos más importantes se representan en la Fig. 10 y la totalidad de los datos en la Tabla 1.*

El contaje de ciclos para las unidades 9–8 es relativamente fácil. La Fig. 11 ilustra este intervalo en las secciones de Zumaia y Sopelana I. Se observan 32 pares litológicos (ciclos de precesión P_K73 to P_K104) que comprenden 6 ciclos relacionados con la excentriciadad nombrados E18 a E23.La Unidad 7 es relativamente margosa y está mejor expuesta en Zumaia (Fig. 12). La observación de los ciclos de excentricidad se realiza sin problemas aunque el ciclo E26 es menos claro. La Unidad 6 se caracteriza por un tramo carbonatado de unos 15 m de espesor con un intervalo margoso pronunciado de 1.2 m hacia la mitad que se ha denominado con el apelativo coloquial "Escalón" (Fig. 13). Aunque las capas margosas del par litológico no estén muy desarrollados se han podido contar 24 ciclos de precesión y 4-5 ciclos de excentricidad en la Unidad 6. El estudio magnetostratigráfico de esta unidad (Fig. 14) ha permitido localizar la inversión C31r/C30n en el ciclo de precisión $P_E20\pm1$. En Sopelana I, también es posible observar los 24 pares litólogicos y localizar la inversión C31r/C30n aunque existe una falla que separa dos bloques (Fig. 15).

En Hendaia la sucesión del Cretácico Superior aflora a lo largo de la Pointe Sainte-Anne en diversos bloques separados por fallas (Fig. 16) y se han podido distinguir todas las unidades litológicas 6–12. El estudio magnetostratigráfico en las unidades 11–12 indica una magnetización secundaria que no permite establecer la magnetostratigrafia al igual que en Zumaia y Sopelana (Fig. 17). En cambio, la Unidad 6 que se ha estudiado en las secciones denominadas Hendaia E y Hendaia W (Fig. 18 y 19) permite observar y contar sin ambigüedades los ciclos de precesión de esta unidad y confirmar la localización de la inversión C31r/C31n.

El límite de cron C31r/C31n (posición estimada a ~3.08 Ma debajo del K/Pg) se ha determinado de forma inequívoca en la parte inferior de la sucesión en las tres secciones estudiadas, pero no ha sido posible determinar el límite de cron C30n/C29r debido a una remagnetización inversa generalizada en las litologías rojizas de la parte superior de la sucesión. Los bioeventos relevantes del plankton calcáreo pueden posicionarse con precisión en el modelo ciclo-magnetostratigráfico. Además, la plantilla ciclostratigráfica (Fig. 20) permite estimar la duración de las secuencias deposicionales de 3er-orden relacionadas con variaciones del nivel del mar que han sido definidas con anterioridad en la cuenca, y que parecen gobernadas por el ciclo de 1.2 Ma de la oblicuidad de modulación de la amplitud.

Introduction

The study of rhythmic sedimentary successions from deep-sea records and on-land outcrops, where a full hierarchy of cyclic stacking patterns has been shown to have originated from astronomical climate forcing on the sedimentary depositional environment, has been central to the development of the modern Geological Time Scale. Astronomical tuning of these sequences to accurate orbital solutions provided by astronomers has led to unprecedented accuracy, resolution and stability in the geological record throughout the earliest part of the Cenozoic, which has benefited from methodological enhancements and improved astronomical models in recent years. Milankovitch climate cyclicity tied to magnetic polarity stratigraphy is the backbone of the recent geological past (Kent, 1999). A notable achievement of this integrated effort was the completion of an astronomical time scale for the Neogene (Astronomically Tuned Neogene Time Scale, ATNTS2004; Lourens *et al.*, 2004), which was incorporated into the GTS2004 Geological Time Scale (Gradstein *et al.*, 2004). Tuning the Palaeogene has become more challenging despite new complete numerical solutions for the solar system (Varadi *et al.*, 2003; Laskar *et al.*, 2004) due to uncertainties and limitations inherent to the chaotic behaviour of the solar system and poor radiometric age control. The Palaeocene hemipelagic successions in the Basque Basin, in particular at Zumaia, has contributed to a heated debate as to the extent of the astronomical time scale for this epoch (Dinarès-Turell, *et al.*, 2003, 2007, 2010, 2012; Westerhold *et al.*, 2008; Kuiper *et al.*, 2008; Hilgen *et al.*, 2010), which is still not fully resolved. This is mainly due to the existence of the so-called Eocene gap in the astronomical time scale, implying that different options had to be proposed for the Palaeocene, the inconsistencies in cycle recognition through the studied records (Hilgen *et al.*, 2010) and the limitations of the orbital solutions. Recent efforts on cyclic deep-sea records (Westerhold *et al.*, 2012) have shed some controversial light on the calibration of the early Palaeogene. In any case it has become clear that very long geological records are needed to overcome some of the limitations inherent in astronomical solutions for geological time intervals older than ~54 Ma, which could potentially provide crucial information for astronomers. Previous attempts to arrive at orbital correlations between Cretaceous successions linked to a time framework including the K/Pg boundary and some magnetic chrons have focused mostly on elapsed time (*cf.* Herbert *et al.* 1995; Herbert, 1999). Only recently has the entire Maastrichtian been tuned to modern astronomical solutions (Husson *et al.*, 2011, Thibault *et al.*, 2012) from the evidence of deep-sea records. We offer here the results of a first comprehensive integrated cyclo- and magnetostratigraphic analysis and study of the calcareous nannofossils within the Upper Maastrichtian succession in the Basque Basin.

Materials and Methods

Studied sections and previous works

The Basque Basin was a deep-water interplate trough (flysch trough) flanked by shallow shelf areas to the north (Aquitania), south (Iberia) and east, and opening westward into the Bay of Biscay (Fig. 1). Throughout the Late Maastrichtian and Palaeocene the sea

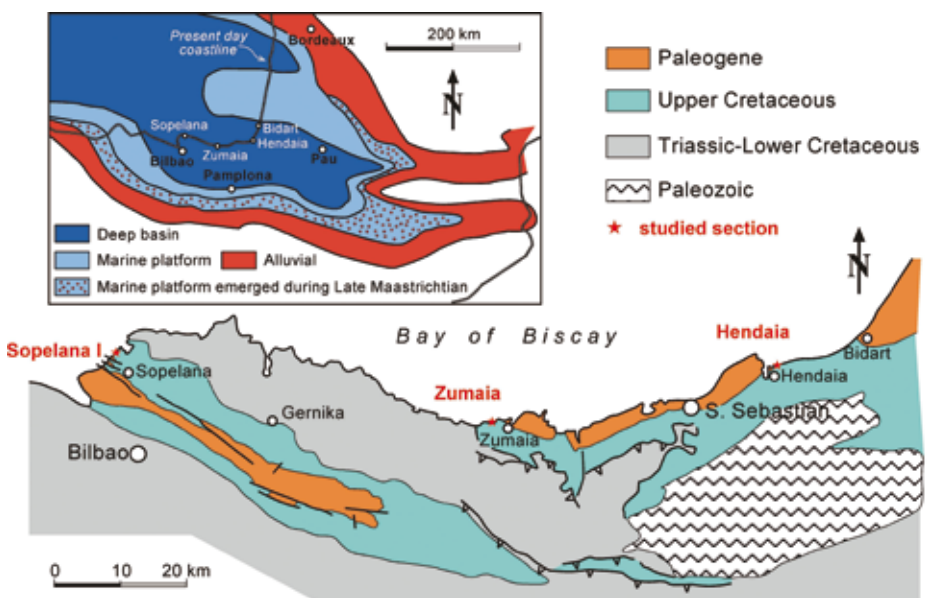

Figure 1. Simplified geological map showing the location of the sections studied in the Basque Basin. The inset is a palaeogeographic sketch of the Pyrenean area showing the distribution of the different depositional settings during the Maastrichtian (modified from Plaziat, 1981).
Figura 1. *Mapa geológico simplificado que muestra la ubicación de las secciones estudiadas en la Cuenca Vasca. El recuadro es un bosquejo paleogeográfico de la zona pirenaica, mostrando la distribución de los ambientes deposicionales durante el Maastrichtiense (modificado de Plaziat, 1981).*

transgressed the shallow flanking areas, leading to the development of extensive ramps, or carbonate platforms (Plaziat, 1981; Pujalte *et al.*, 1994; Baceta *et al.*, 2004). This wholesale transgression also made it difficult for coarse-grained siliciclastic deposits to reach the deep trough, which became the site of a hemipelagic limestone/marl type of sedimentation, with turbidites being mainly restricted to the base of the slope area (Fig. 1).

The Maastrichtian succession from the Basque Basin crops out best along different coastal exposures (i.e. Zumaia and Sopelana, separated by about 70 km), which have usually been studied mainly for their biostratigraphic content, such as ammonites, inoceramids and calcareous plankton (Herm, 1963; Lamolda, 1985; Ward *et al.*, 1986, 1991; Wiedmann, 1988; MacLeod and Orr, 1993; Ward and Kennedy, 1993; Burnett *et al.*, 1992; MacLeod, 1994; Lamolda and Gorostidi, 1994; von Hillebrandt, 1965; Arz and Molina, 2002). Other studies include carbon and oxygen stable isotopes (Mount and Ward, 1986; Gómez-Alday *et al.*, 2004, 2008; Paul and Lamolda, 2007). The orbital origin of the limestone/marl alternations has also been explored (Mount and Ward, 1986; Ten Kate and Sprenger, 1993). Magnetostratigraphy for the Upper Maastrichtian had only been published for the Sopelana section (Mary *et al.*, 1991). More recently a multidisciplinary calcareous plankton and magnetostratigraphic study of the Maastrichtian in the Zumaia section was undertaken (Pérez-Rodríguez *et al.*, 2012) but no detailed lithological log or cycle counting was provided.

The bulk of the Maastrichtian strata correspond to the Zumaia-Algorri Formation (Mathey, 1982) and consist of alternations of hemipelagic limestones and marls and subordinate clay-shales, and in some sections thin- to medium-bedded (cm to dm thick) turbidites. On the basis of the varying proportions of these lithologies, a lithostratigraphic subdivision into formal members (Member I to V of Ward, 1988; Ward and Kennedy, 1993) and more detailed informal lithological units (Units 2 to 12 of Wiedmann, 1988) have been commonly used (Fig. 2). These lithological units can generally be recognised in widely separate sections, from Sopelana in the west to Bidart in the east (Fig. 1), although individual unit thickness, rock colour and number and the thicknesses of the turbidite beds are variable. At about 240 m the Maastrichtian succession at Zumaia is the thickest (Fig. 2) and can be taken as representative. The oldest member corresponds to pale-grey, limestone-marl alternations (Member I) and has been subdivided into 4 units (Units 2 to 5) based on their relative carbonate content, thickness and frequency of turbidite beds, and overall erosion expression in the field. Member II (Unit 6) is dominated by pale limestones containing a conspicuously darker metre-scale marl bed in the middle that has been colloquially termed "Escalón" (= step or indentation). According to the most recent study of the integrated calcareous nannoplankton and magnetostratigraphic in the Zumaia section (Pérez-Rodríguez *et al.*, 2012) the Lower/Upper Maastrichtian boundary interval is located in Unit 6. Member II is overlain by a marlstone unit (Member III), distinctive because of its reddish to chocolate-brown colour. The overlying unit (Member IV) is formed by limestone-marlstone rhythmites and is subdivided into 4 subunits: relatively carbonate-rich pale gray Units 8-9, followed by reddish marly-rich Unit 10 and relatively carbonate-rich Unit 11. The last Maastrichtian Member (V) is a deep-purplish marly unit (Unit 12). Later authors interpreted these large-scale alternations in terms of sequence stratigraphy, recognizing 3 successive 3rd-order depositional sequences in the upper Maastrichtian-lowest Danian interval (Fig. 2). Thus, Pujalte *et al.* (1995), on the basis of the classic model of Posamentier and Vail (1988), attributed the marl-dominated units to the low-stand fan system tract (LSF) and the limestone-marl rhythmic units to the low-stand wedge and high-stand system tracts (LSW + HST) within the 3rd-order depositional sequence (DS-1, DS-2.1 and DS-2.2, from older to younger). Baceta *et al.* (2004), although agreeing in their characterization, renamed these sequences Ma-1, Ma-2 and Ma-Da and, following a more conservative approach, did not subdivide them into system tracts. We have renamed these sequences, inverting the numbering (UMa-2, UMa-1 and UMa-Da, from older to younger), thus allowing for potential extension into older ages and trying to reconcile previous interpretations by simply using low- and high-stand system tracts (Fig. 2). Despite the different terminology the rationale for both interpretations is similar. In brief, marl-dominated units were assigned to periods of relatively low sea-level, based upon the argument that during these intervals the shoreline would be nearer, making it easier for fine-grained clastic deposits to reach the deep basin (see Units 7, 10 and 12 in Fig. 2). Conversely, a high sea-level would hinder the arrival of clastic sediments and facilitate the accumulation of the hemipelagic limestones that characterize Units 9-8, and 11, and also the lower part of the Danian succession (Fig. 2).

In this study we have focused on the interval comprising Units 6 to 12, which encompass 3 sections of the Upper Maastrichtian: Zumaia, Sopelana I, and Hendaia (Fig. 1). The Upper Maastrichtian Zumaia (base of section 43°17'56.31"N/2°16'09.03"W) and the Sopelana I (base 43°23'19.06"N/2°59'39.29"W) coastal-cliff sections constitute the primary sections studied (Fig. 3).

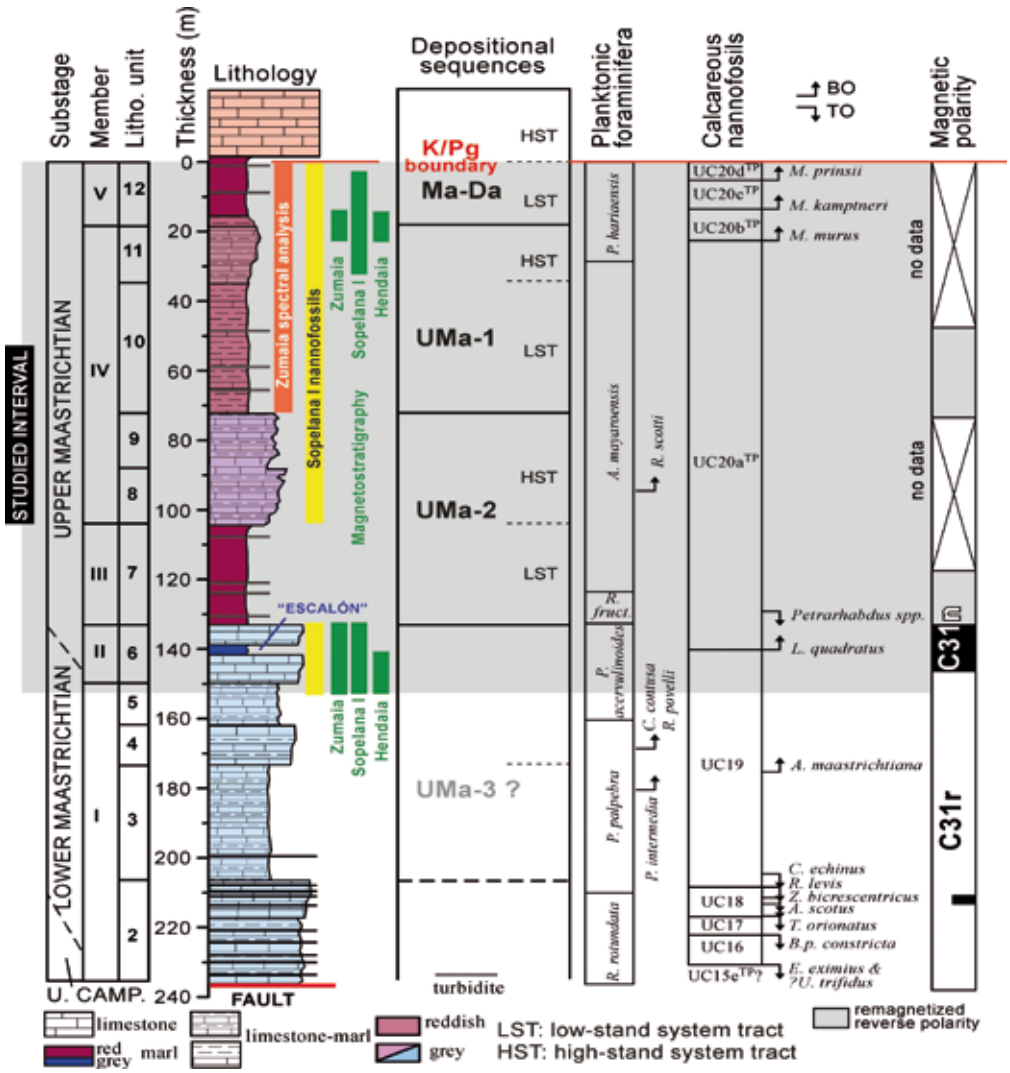

Figure 2. Synthetic stratigraphic log of the Maastrichtian succession (based on the Zumaia section) in the Basque Basin. The lithological Units U5–U12 of Wiedmann (1988) and Members I–V of Ward (1988) are indicated. The most recent calcareous plankton biostratigraphy and magnetostratigraphic results at Zumaia are depicted (Pérez-Rodríguez *et al.*, 2012).

Figura 2. *Columna estratigráfica sintética de la sucesión Maastrichtiense (basada en la sección de Zumaia) en la Cuenca Vasca. Se indican las unidades litológicas U5–U12 de Wiedmann (1988) y los miembros I–V de Ward (1988). Se representan los resultados biostratigráficos publicados más recientes de plancton calcáreo y magnetostratigrafía de Zumaia (Pérez-Rodríguez* et al.*, 2012).*

The Upper Maastrichtian at Zumaia (Units 6–12, ~150 m) is comprised of limestone-marl alternations, including hundreds of thinly bedded turbidites. The Upper Maastrichtian succession at Sopelana I (~70 m) has the advantage that it lacks interbedded turbidites. This succession is, on the other hand, relatively tectonized and not straightforward to follow in detail at first glance, despite the fact that main lithological units can be identified (Fig. 3b). Nevertheless, careful observations and resolution of some complex faults lead to a proper recognition and a bed-by-bed correlation with the precession cycles identified at Zumaia (see below). Zumaia, besides being the thickest section, represents a key area in the stratigraphic analysis of the Upper Cretaceous and Palaeocene. Extensive, integrated, high-resolution chronostratigraphic studies, including astronomical tuning, have been undertaken for the Palaeocene part (Dinarès-Turell *et al.*, 2002, 2003, 2007, 2010, 2012; Kuiper *et al.*, 2008) and the section hosts the two internal Palaeocene Global Standards Section and Points (GSSPs) at the base of the Thanetian and Selandian stages (Schmitz *et al.*, 2011) and an auxiliary K/Pg boundary (Molina *et al.*, 2009). Moreover, a high-resolution carbonate record for the Upper Maastrichtian Units 10–12 had been published previously and analysed for astronomical purposes (Ten Kate and Sprenger, 1993). Therefore it seemed rational to extend the astronomical observations to older ages and potentially

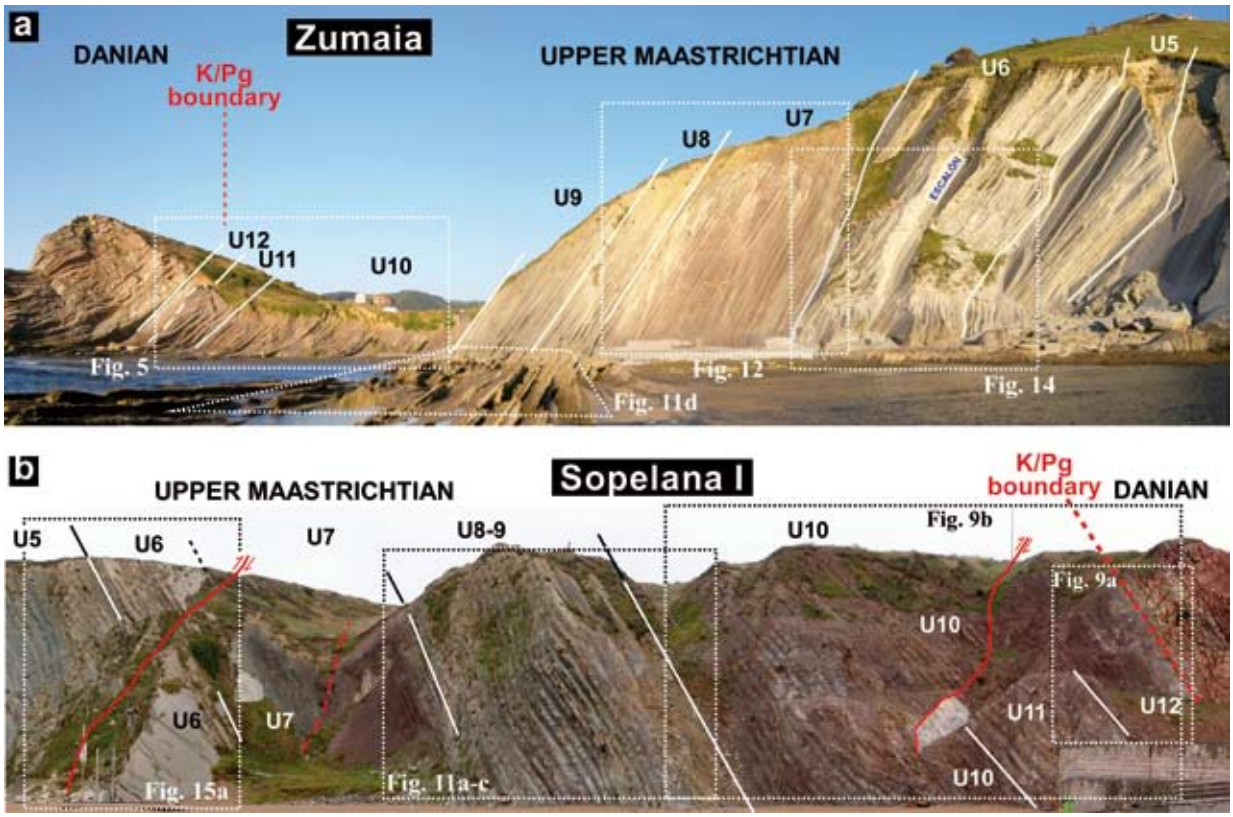

Figure 3. Panoramic views of the Upper Maastrichtian strata from the coastal-cliff exposures at Zumaia (a) and Sopelana I (b). The lithological units of Wiedmann (1988) and the location of several figures are indicated.
Figura 3. *Vistas panorámicas de la sucesión del Maastrichtiense Superior en los acantilados costeros de Zumaia (a) y Sopelana (b). Se indican las unidades litológicas de Wiedmann (1988) y la ubicación de varias figuras.*

achieve a long, complete astronomical tuning from land-based sections comprising the Maastrichtian that has also recently been astronomically tuned from deep-sea records (Husson *et al.*, 2011, Thibault *et al.*, 2012). We used the bulk carbonate record from Units 10 to 12 at Zumaia taken from Ten Kate and Sprenger (1993) to conduct a new spectral analysis. Magnetostratigraphic data from Zumaia had not been available until recently, but with limited success due to a pervasive remagnetization in the reddish lithologies (Pérez-Rodríguez *et al.*, 2012), whereas an apparent reasonable magnetostratigraphy down to chron C31r had been established in the Sopelana I section (Mary *et al.*, 1991), although complex magnetization mechanisms were invoked for the section (Moreau *et al.*, 1994). Consequently we undertook a palaeomagnetic study at Sopelana I and Zumaia to reproduce the earlier magnetostratigraphy on a suitable cyclostratigraphic framework. Furthermore, we have produced an extensive, high-resolution, calcareous nannofossil biostratigraphy for the first time throughout the Sopelana I section.

We also explored other Upper Maastrichtian sections at Hendaia that present certain lithological peculiarities. After recognising the standard lithological units and identifying the cycles we targeted relevant intervals within the Maastrichtian outcrops along the coastal-cliffs of Pointe Sainte-Anne near Hendaia for magnetostratigraphic purposes. Three nearby outcrops were examined: the Hendaia E section (3°22'56.36"N/0°45'16.97"W) for the C31r/C31n reversal in Unit 6 and the Hendaia N section (43°23'03.00"N/1°45'09.64") for the chron C30n/C29r reversal close to the contact between Units 11 and 12. Some additional observations were made in Unit 6 in the Hendaia W outcrop.

Magnetostratigraphy

Hand-samples for palaeomagnetic analysis where taken and oriented *in situ* with a magnetic compass before cutting standard cubic specimens in the laboratory for analysis. We aimed at a high-resolution chronostratigraphic framework so sampling was done at a lithological couplet level (~21 ky resolution). Only relevant intervals within the studied sections were sampled for magnetostratigraphic purposes. These included the chron C30n/29r reversal around the boundary of Units

11/12 at Zumaia (16 beds), Sopelana I (43 beds) and Hendaia (9 beds), and the C31r/C31n reversal in Unit 6 at Zumaia (33 beds), Sopelana I (13 beds) and Hendaia (10 beds). Natural remanent magnetization (NRM) and remanence through demagnetization were measured on a 2G Enterprises DC SQUID high-resolution pass-through cryogenic magnetometer (manufacturer noise level of 10^{-12} Am^2) operated in a shielded room at the Istituto Nazionale di Geofisica e Vulcanologia in Rome, Italy. A Pyrox oven in the shielded room was used for thermal demagnetization and alternating field (AF) demagnetization was done with three orthogonal coils installed in line with the cryogenic magnetometer. Progressive stepwise AF demagnetization was routinely used and applied after a single heating step to 150°C. AF demagnetization included 14 steps (4, 8, 13, 17, 21, 25, 30, 35, 40, 45, 50, 60, 80, 100 mT). Samples that did not fully demagnetize after this protocol were further demagnetized thermally and a number of samples were demagnetized using thermal treatment alone. Characteristic remanent magnetizations (ChRM) were computed by least-squares fitting (Kirschvink, 1980) on the orthogonal demagnetization plots (Zijderveld, 1967).

Calcareous nannofossils

The nannofossil content of 76 samples was analysed within the Upper Maastrichtian of the Sopelana I section from the K/Pg boundary down to the lower part of Unit 6 (~67 m total thickness). No samples were collected in Unit 7 as it is tectonized and most probably incomplete. The sampling resolution strategy was aimed at obtaining complete nannofossil data for every marl-limestone couplet to pinpoint precisely the main Upper Maastrichtian nannofossil biohorizons. A small chip of the rock sample was processed and fixed on a smear slide following the standard preparation technique (Bown and Young, 1998) in order to preserve the original species composition. The nannofossil was studied under a Zeiss Axioscop 40 microscope at magnification 1250 X. Photographs were taken with a ProgRes GT3 camera and its corresponding software. Three long traverses were logged on each slide and the relative abundance of nannofossils was recorded semi-quantitatively using standard categories: Common (C), 1–10 specimens per field of view (fov), Frequent/Few, 1 specimen <20 fov; Rare, 1 specimen >20 fov.

The calcareous nannofossil biozonation for the Upper Maastrichtian used here is primarily based on the UC scheme of Burnett (1998), but the previous CC biozonation of Sissingh (1977) and Roth (1978), as emended by Perch-Nielsen (1985), is also taken into account (Fig. 4). The taxonomic concepts generally follow those of Perch-Nielsen (1985) and Burnett (1998), but some recent emendations are also applied (Lees and Bown, 2005; Lees, 2007; Thibault, 2010). The taxonomic characterization of all species can be found at www.nannotax.org.

Spectral analysis and orbital solutions

The Zumaia bulk carbonate record for Units 10, 11 and 12 according to Ten Kate and Sprenger (1993) was used for spectral analysis. The original dataset was collected at intervals of 10 cm throughout the 63.7 m succession, in which many thin bedded turbidites ranging from 0.1 to 12 cm interbedded within the rhythmic hemipelagic marl-limestone couplets can be recognised. The published record was digitized and resampled at 10 cm intervals prior to spectral analysis. Ten Kate and Sprenger (1993) followed a strategy to tune the record

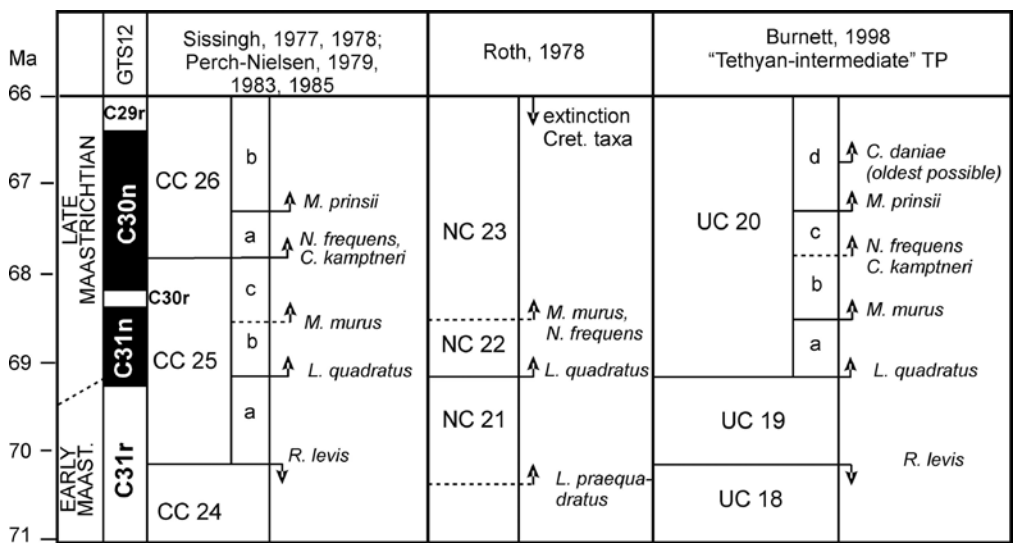

Figure 4. Upper Maastrichtian calcareous nannofossil zonations through the GTS2012 (Gradstein *et al.*, 2012).

Figura 4. *Zonaciones de nannofósiles calcáreos para el Maastrichtiense Superior a través de la GTS2012 (Gradstein* et al.*, 2012).*

to the theoretical eccentricity curve available at the time (Berger, 1978), extrapolated to 65 Ma. The procedure started with a strong smoothing of the carbonate record using a weighted three-point moving average a number of times on a 2.5 cm interpolated spline curve fitted though the original data points. It proceeded by making firstly a visual correlation of the minima in the record and the target curve. Correlation was subsequently refined by the assessment of other smaller scale features. Spectral analysis was then performed on the time domain to conclude that the carbonate rhythmicity is indeed orbitally controlled as power on the precession and eccentricity bands was observed. The authors recognised that extrapolating the Berger's equation to 65 Ma was unacceptable because of inaccuracies in the solution that could amount to 0.4 Ma and therefore any absolute chronological constraints had to be flawed. We also note that correlating the eccentricity minima to low carbonate minima clashes with the observed details of cycle pattern recognition that suggests an opposite phase. In fact, as has been observed for the Palaeocene interval, precession-related cycles are less well developed in the limestone-dominated intervals of eccentricity-related cycles, indicating that these beds do indeed correspond to eccentricity minima because eccentricity modulates the precession signal's amplitude (Dinarès-Turell *et al.*, 2003, 2010, 2012; Kuiper *et al.*, 2008). Consequently, the approach we have followed to analyse the carbonate record from Zumaia is different. We first conducted spectral analysis in the depth domain and inferred the astronomical frequencies and periods. Subsequently, we extracted the orbital cycles from the record by using bandpass Gaussian filters centred on the significant periodicities. The standard (Fourier) spectra was calculated using the software package "AnalySeries" (Paillard *et al.*, 1996), which was also been employed for filtering purposes. The Continuous Wavelet Transform (hereafter CWT) (Torrence and Compo, 1998), which has been divided by its scales to account for a bias in the power spectrum (Liu *et al.*, 2007), was also applied to analyse the time evolution of the spectral power and to visualize better the eccentricity amplitude modulations on the precession.

Modern astronomical solutions that include a direct numerical integration of planetary orbits and the precession of the Earth's spin axis include the orbital solutions Va03_R7, published by Varadi *et al.* (2003), and La2004, by Laskar *et al.* (2004). The Va03_R7 solution was first used to tune the Danian portion of the Zumaia section (Dinarès-Turell *et al.*, 2003) whereas the La2004 solution has since predominated in the literature and been used to tune the Neogene (Lourens *et al.*, 2004) in the GTS2004 geological time scale (Gradstein *et al.*, 2004). Due to the chaotic behaviour of the solar system the orbital solution cannot be accurately calculated beyond 40 Ma (Laskar *et al.*, 2004), and therefore only the stable 405-ky eccentricity cycles can be used for tuning purposes. In an effort to improve the accuracy of the astronomical solution beyond 40 Ma a new solution (La2010) has recently been put forward (Laskar *et al.*, 2011a) that makes use of a new high-precision planetary ephemeris called INPOP. In fact four solutions have been proposed, La2010a, b, c, d, which are adjusted in a different manner with the scope to assess the long-term precision of the solutions, which still maintained only limited accuracy beyond ~60 Ma (Laskar *et al.*, 2011a). Further developments in ephemeris precision and methodological computations have led to yet another solution, La2011 (Laskar *et al.*, 2011b), which provides slight refinements to the previous solutions. Nevertheless, Laskar *et al.* (2011b) demonstrate that the motion of Ceres and Vesta is very chaotic. As a consequence, a precise calculation of Earth's eccentricity beyond 60 Ma is at present impossible, and probably never will be (*cf.* Westerhold *et al.*, 2012 for additional details). A stability test on the La2010 and La2011 orbital solutions carried out by Westerhold *et al.* (2012) suggests that only the La2010d and La2011 solutions should be used beyond ~47 Ma. In conclusion, it remains clear that for the Maastrichtian an accurate tuning for the short eccentricity is not possible and only the 405-ky beat can be used for that purpose. Only continuous, very long, astronomically forced geological records could shed light on the orbital configuration at these older time scales. Our scope in this paper is not to look in detail at the tuning options but just to present a cyclostratigraphic template among the different Upper Maastrichtian sections from the Basque Basin for further future developments.

Results

The integrated cyclostratigraphic, magnetostratigraphic and biostratigraphic results are presented for both the Zumaia and Sopelana I main sections in inverse stratigraphic order following the lithological units of Wiedmann (1988) from younger Units 12–10 to older Units 9–7. The results from the accessory Hendaia section are presented separately at the end.

Units 12–10

Units 12–10 are magnificently exposed at the coastal-cliff of Punta Aitzgorri in Zumaia (Figs. 5a-c), which is reachable on foot at low-tides. The succession is also

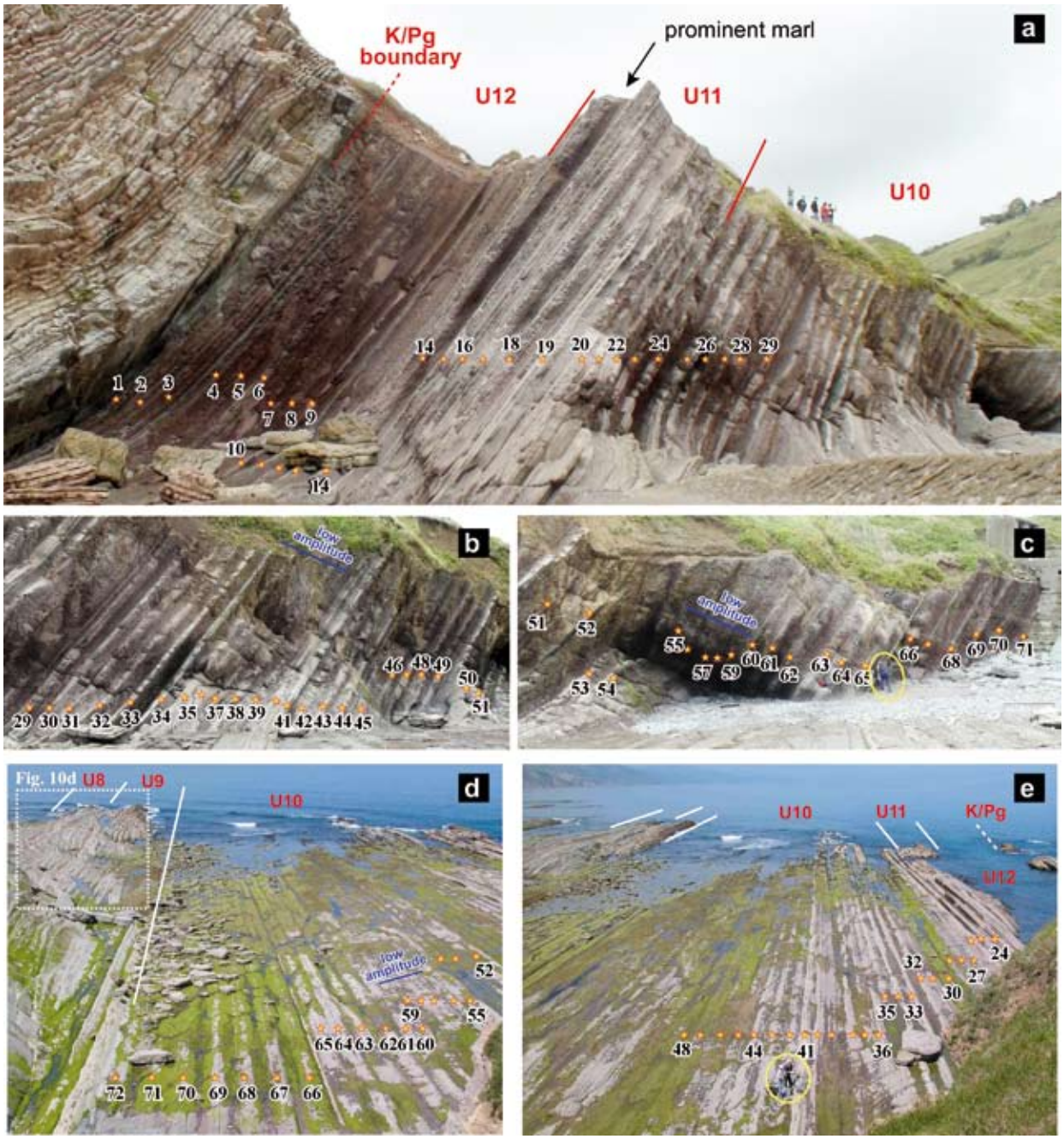

Figure 5. Field photographs of Maastrichtian Units 10–12 at the coastal-cliff (a-c) and major wave-cut platform (d-e) exposures at Zumaia, in which individual precession-related couplets have been numbered (see P_K1 to P_K72 in text).
Figura 5. *Fotografías de campo de las Unidades 10–12 del Maastrichtiense en los acantilados costeros (a-c) y afloramientos de la rasa mareal (d-e) en Zumaia, donde los pares litológicos relacionados con la precesión han sido numerados (ver P_K1 a P_K72 en el texto).*

exposed on the wave-cut platform during very low tides (Figs. 5d, e) and the marl-limestone couplets are relatively easy to recognise with the exception of the couplets within Unit 12 below the K/Pg boundary due to their generally more marly character and the presence of very thin interbedded turbidites. In a good light at low tide the couplets can clearly be distinguished. The lithological couplets have been numbered from the K/Pg downward and consist of a marly layer at the bottom and a carbonate-rich bed at the top. A total of 72 basic couplets with an average thickness of around 0.9 m have been recognised throughout the interval under consideration. The first three couplets (1–3) just below the K/Pg are relatively thick and carbonate rich. Couplets 6 and 9–10 also are carbonate-rich. Couplets 11–13 are somewhat more difficult to recognise because

they are thin and relatively homogeneous. Then, a very characteristic prominent marl bed is found in couplet 14. Below this level the couplets are easy to recognise down to the base of Unit 10 and open bundles of about 5 couplets can eventually be observed. Furthermore, some intervals of relatively low-amplitude limestone-marl couplets seem to be visible (intervals of cycles 35–39 and 55–60) (Figs. 5b, c).

A high-resolution carbonate record had previously been produced and analysed to evaluate astronomical forcing in Units 10–12 (Ten Kate and Sprenger, 1993),

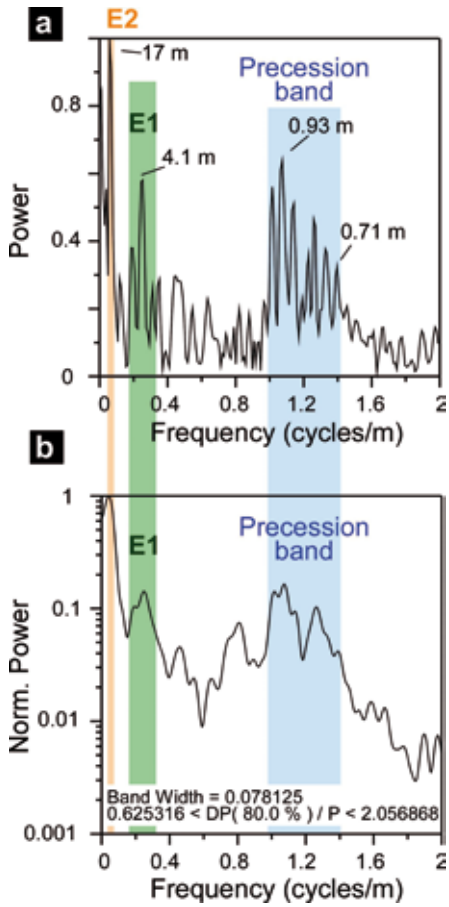

Figure 6. Spectral analysis of the carbonate data series of the Zumaia section comprising Units10–12. a) Periodogram using a Barlett window; and b) Blackman-Tukey power spectra with a Barlett window carried out with the AnalySeries v.2 software package (Paillard *et al.*, 1996). Significant peaks or bands are labelled or marked by shaded bands; the period in m is also given. Inferred Milankovitch components are represented by E2 (long eccentricity, ~405-ky), E1 (short eccentricity, ~100-ky), and precession band (~19-23 ky).

Figura 6. *Análisis espectral de la serie de datos de carbonato de la sección de Zumaia que comprende las Unidades 10–12. a) Periodograma utilizando una ventana de Barlett; y b) espectros Blackman-Tukey y una ventana de Barlett llevados a cabo con el software AnalySeries v.2 (Paillard* et al.*, 1996). Picos y bandas significativas se han etiquetado o marcado con sombreados; también se indica el período en m. Los componentes de Milankovitch deducidos están representados por E2 (excentricidad larga, ~ 405-ka), E1 (excentricidad corta, ~ 100-ka) y la banda de la precesión (~ 19-23 ka).*

demonstrating that indeed the lithological couplets in the Maastrichtian also represent precession cycles of ~21-ky duration. Here we take the same record and perform the spectral analysis in the depth domain in order to extract the precession and the short (~100-ky) and long (~405-ky) eccentricity-related periodicities. Three distinct periodicities can be distinguished on the standard Fourier periodogram (Fig. 6a) and Blackman-Tukey spectrum (Fig. 6b). A band of significant frequencies with periods at 0.7-0.95 m is associated with the couplet and related to precession. A period at 4.1 m is related to the short eccentricity whilst a narrow period at 17 m, which appears blurred on the Blackman-Tukey spectrum, can be associated to the 405-ky long eccentricity. Figure 7a shows the distribution of the precession cycles (i.e. the 72 marl-limestone couplets named P_k1 to P_k72), and the short and long eccentricity cycles through Units 12–10 at Zumaia. The CWT spectrum (Fig. 7b) allows us to visualize the spacial evolution of these periodicities, which also emerge on the global spectrum. It appears clear that the precession band within the lower stratigraphic interval (52–64 m) is shifted to slightly higher periods due to the presence of relatively thicker couplets in this interval (Fig. 5d). Another advantage of the CWT spectra is the ability to display variations in the overall amplitude within a certain band. As it is known that eccentricity modulates precession the CWT spectra become a useful tool for unravelling this scenario, since the overall significance of the eccentricity power in the standard spectra may be depleted under a strong precession forcing on the sedimentary record (*cf.* Dinarès-Turell *et al.*, 2012). The precession band on the CWT spectrum (Fig. 7b) shows three zones of relatively lower amplitude. They are clearly associated to the 405-ky long eccentricity minima that we have named $Ma_{405}1$, $Ma_{405}2$ and $Ma_{405}3$ from the K/Pg boundary downward, following the terminology used by Westerhold *et al.* (2008) and Husson *et al.* (2011), although these authors numbered the eccentricity maxima instead. Gaussian bandpass filters centred at the retrieved periods have been used to extract the orbital cycles from the carbonate record (Fig. 7a). The ~100 ky eccentricity minima have also been numbered from the K/Pg downward. A total of 17 short eccentricity cycles have been recognised through the interval comprising Units 10–12 (named E1 to E17). It should be noted, however, that cycles E3 and E4 are less well defined whereas cycles E16 and E17 appear to contain less than the usual 4–6 precession cycles, which may be an artefact of the higher sedimentation rate during this interval, and consequently the number of eccentricity cycles might be overestimated.

No magnetostratigraphic results for the Maastrichtian Units 12–10 at Zumaia have ever been published

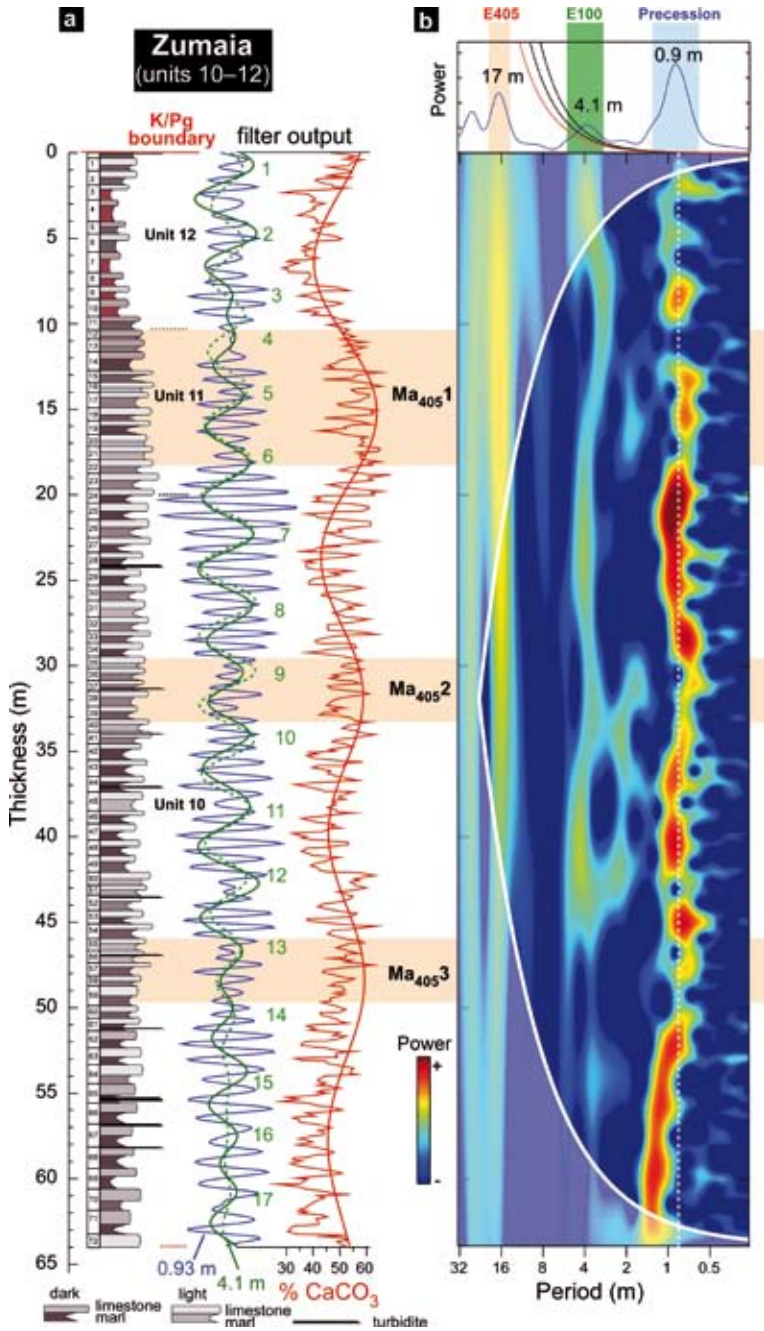

Figure 7. a) Detailed lithological log for Units 10–12 from Zumaia and the corresponding carbonate ($CaCO_3$) record of Ten Kate and Sprenger (1993). The filter output of Gaussian filters centred at 0.93 m (blue line, 1.074±0.5 bandpass), 4.1 m (solid green line, 0.244±0.06 bandpass; dashed green line, 0.244±0.02) and 17 m (red line, 0.058±0.015 bandpass) are also shown. The precession-related lithological couplets are numbered from the K/Pg boundary downward throughout the log (P_K1 to P_K72). The green numbers indicate lithological bundles corresponding to the short-eccentricity (100 ky) minima and the black labels indicate the long eccentricity (405 ky) minima (Ma_{405}) relative to the K/Pg boundary. b) Wavelet and global power spectrum with a lag-1 red-noise estimate and respective 80% and 95% significance levels.

Figura 7. *a) Columna litológica detallada para las Unidades 10–12 de Zumaia y el correspondiente registro de carbonato ($CaCO_3$) de Ten Kate y Sprenger (1993). Se muestra también el resultado de filtros Gaussianos centrados en 0.93 m (línea azul, pasabanda de 1.074±0.5), 4.1 m (línea verde continua, pasabanda 0.244±0.06; línea verde discontinua, 0.244±0.02) y 17 m (línea roja, pasabanda de 0.058±0.015). Los pares litológicos se numeran desde el límite K/Pg hacia abajo a lo largo de la sucesión (P_K1 a P_K72). Los números verdes indican paquetes litológicos correspondientes a mínimos de la excentricidad corta (100 ka) y las etiquetas negras indican mínimos de la excentricidad larga (405 ka) (Ma_{405}) en relación con el límite K/Pg. b) Espectro continuo de ondas y espectro de energía global con una estimación lag-1 del ruido rojo y niveles respectivos de significancia del 80% y 95%.*

despite several attempts by different researchers (Ten Kate and Sprenger, 1993; Verosub, personal communication 2000). In fact, Ten Kate and Sprenger (1993) quote an unsubstantiated layer by layer correlation of the Zumaia and Sopelana successions, for which the available magnetostratigraphic study at Sopelana (Mary *et al.*, 1991) was used to infer the position of the chron reversal "C30R/C31N" (as it is quoted originally) at "12.3 m below the sampled interval" at Zumaia (one should understand in Unit 9). This depth seems to have been used to place the C30n/C29r position at Zumaia by Westerhold *et al.* (2008) (and probably Herbert *et al.*, 1995), whilst it is clear that Ten Kate and Sprenger were referring to a reversal translated at 74.75 m below the K/Pg boundary at Zumaia (see their Table 1). Overall, this is quite confusing because Herbert *et al.* (1995) depict the Zumaia carbonate record of Ten Kate and Sprenger (1993) along with the inferred/translated magnetostratigraphy from Sopelana and claim to count 18 precession cycles for the Maastrichtian part of chron C29r, which is close to their inferences for South Atlantic deep-sea records of 18.5

cycles. In any case, Herbert *et al*. (1995) and Herbert (1999) indicate that the C30n/C29r reversal appears to be located close to a node of low-amplitude precession cycles related to the 405-ky eccentricity minima. This was also deduced by Westerhold *et al*. (2008), who infer it close to the minimum between their Ma_{100}-4 and Ma_{100}-3 short eccentricity cycles, although the inferences by these authors concerning Zumaia-Sopelana may be flawed in detail. Mary *et al*. (1991) did not report any reference to cyclicity counting at Sopelana and they only report the C30n/C29r chron boundary at 8 m below the K/Pg boundary. While we report here in our study a comprehensive bed-by-bed correlation and cycle counting between Zumaia and Sopelana, we have revisited and report new magnetostratigraphic data aimed at reproducing the original data from Sopelana. Recent palaeomagnetic data by Pérez-Rodríguez *et al*. (2012) from the lower part of Unit 10 at Zumaia has confirmed the earlier notion on the difficulty of retrieving a primary useful magnetic signal there. Here we provide demagnetization data from Unit 11 throughout the stratigraphic interval where the C30n/C29r boundary should be placed (Fig. 8). In essence, our combined thermal and AF demagnetization protocol leads us to infer a somewhat complex scenario of a reversed remagnetization present in both the magnetite and hematite fractions. In particular, the hematite unblocks at relatively low-temperatures (from 300°C to about 640°C), suggesting a secondary chemical origin. Samples from precession cycles P_K14 (Fig. 8b) and P_K16 (Fig. 8e) display a normal component blocked on hematite and magnetite respectively but the majority of samples only present a pervasive reverse component retaining secondary remagnetization, as was inferred for Unit 10 by Pérez-Rodríguez *et al*. (2012).

Careful observations have been made at the Sopelana I section in Units 12–10 below the K/Pg boundary that were facilitated by the dismantling of some buildings that partly obstructed the cliff outcrops. Some complex faults render it difficult at first glance to follow the cyclic pattern, but we have been able to reconstruct a continuous section that expands Units 12–10 through two partly overlapping faulted blocks (Fig. 9) and to recognise the 72 marl-limestone couplets (i.e. precession cycles P_K1 to P_K72) first seen at Zumaia, including all the lithological particularities and the cyclostratigraphic stacking pattern (e.g. relatively carbonate-rich cycles P_K6, and P_K9–10 and the prominent marl at cycle P_K14, among others). It is noteworthy that the Maastrichtian succession at Sopelana I lacks turbidites.

A thorough magnetostratigraphic study of Units 12–10 has been done, focusing particularly on Unit 11 with the aim of relocating precisely the C30n/C29r chron boundary. We also conducted for the first time a high-resolution survey of the calcareous nannofossils in this section (Fig. 10). Palaeomagnetic results very much resemble our findings at Zumaia. A pervasive reverse overprint seems to be present throughout the studied interval, blocked either in magnetite and/or hematite, as deduced from the combined thermal/AF de-

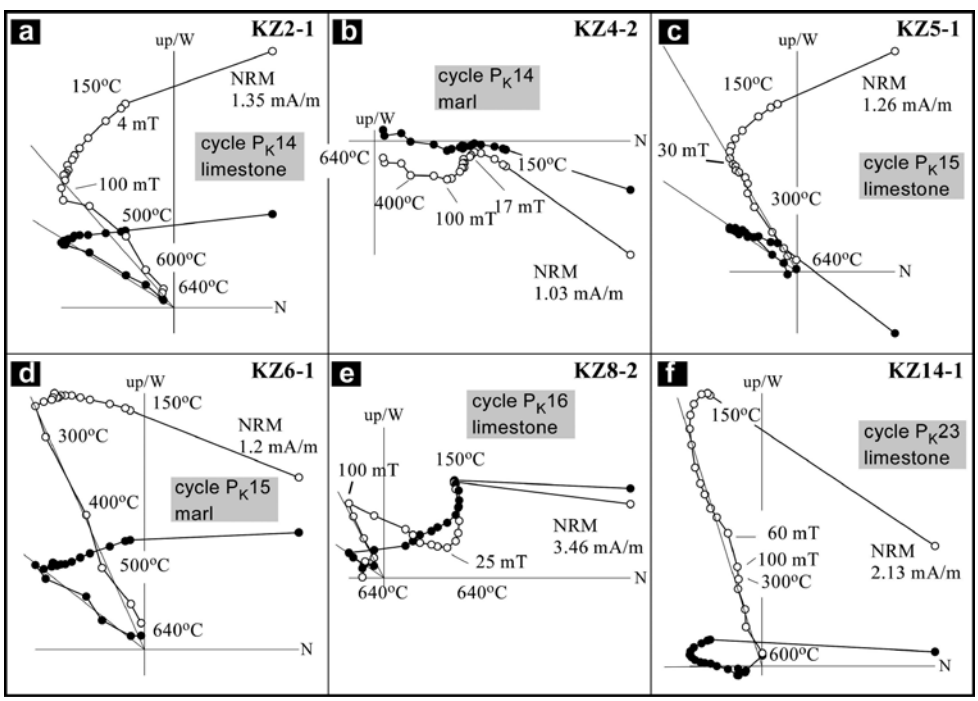

Figure 8. Examples of representative orthogonal demagnetization diagrams in bedding-corrected co-ordinates of Unit 11 at Zumaia (open and solid symbols denote projections onto the vertical and horizontal planes respectively). The precession cycle (P_K), the NRM intensity and some demagnetization steps are indicated.

Figura 8. *Ejemplos representativos de diagramas de desmagnetización ortogonal después de la corrección de capa de la Unidad 11 en Zumaia (símbolos vacíos o rellenos denotan proyecciones sobre los planos vertical u horizontal respectivamente). Se indican el ciclo de precesión (P_K), la intensidad de la NRM y algunos pasos de desmagnetización.*

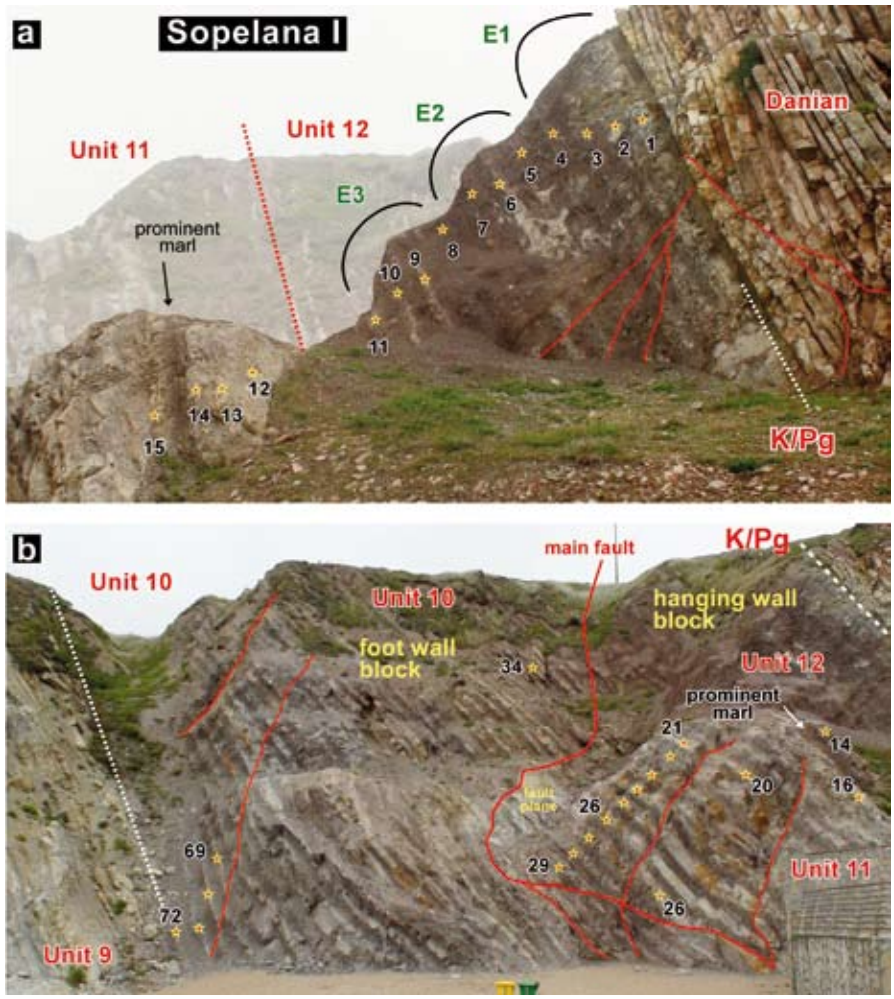

Figure 9. Field photographs for Maastrichtian Units 10–12 at the Sopelana I section. Marl-limestone couplets (i.e. precession cycles, Pk1 to Pk72) and some bundles (i.e. short eccentricity cycles E1–E3) are indicated.
Figura 9. *Fotografías de campo de las Unidades 10–12 en la sección de Sopelana I. Se indican los pares marga-caliza (ciclos de precesión, Pk1 a Pk72) y algunos paquetes (ciclos de excentricidad corta E1–E3).*

magnetization protocol (samples SM5A, SJ69-1A, Fig. 10b). It is noted that thermal demagnetization only on a sister sample (sample SJ69-1B, Fig. 10b), does retrieve what seems to be a spurious component, most probably due to an overlap of the unblocking temperatures of the two components, clearly seen on the combined protocol (sample SJ69-1A, Fig. 10b). This provides evidence of the intricate nature of the magnetization of these reddish rocks and may explain some of the results reported in Mary *et al.* (1991) and Moreau *et al.* (1994). Strikingly, a narrow zone of normal polarity (e.g. sister samples SO-2A and SO-2B, Fig. 10) is found within cycles P_K4–P_K6 that seems to coincide with some awkward directions reported by Mary *et al.* (1991) at 2–5 m below the K/Pg boundary, which they related to plasticity and deformation in these marly lithologies. Although isolated samples with normal polarity have been measured within Unit 11 (see the declination and inclination log, Fig. 10a), no clear picture regarding an unambiguous definition of chron C30n and hence of the C30n/C29r chron boundary could be established. Collectively, the dataset from Zumaia and Sopelana casts some doubts on the earlier interpretations and we regard the magnetization of the reddish lithologies from the Maastrichtian succession to be too complex and unsuitable for magnetostratigraphic purposes.

Calcareous nannofossils are abundant throughout the studied Upper Maastrichtian succession and represented by highly diverse associations showing good to very good preservation. The first occurrence (FO) of *Micula murus* (Plate I, 12) is found in Sopelana at precession cycle P_k41 below the K/Pg boundary (~861 ky below; Fig. 10) (see Table 1 for a full account of bioevents). It is interesting to point out that this primary biotic datum is recorded just 5 m (11 precession cycles = ~231 ky) below the FO of *M. prinsii*. The acme of *M. murus* is observed up-section, within the *M. prinsii* zone. Calibration of these two biohorizons to the magnetic polarity scale and constraining the accurate age by integrated cyclostratigraphy is very important to an evaluation of their biostratigraphic potential, bearing in mind that previous studies have clearly shown

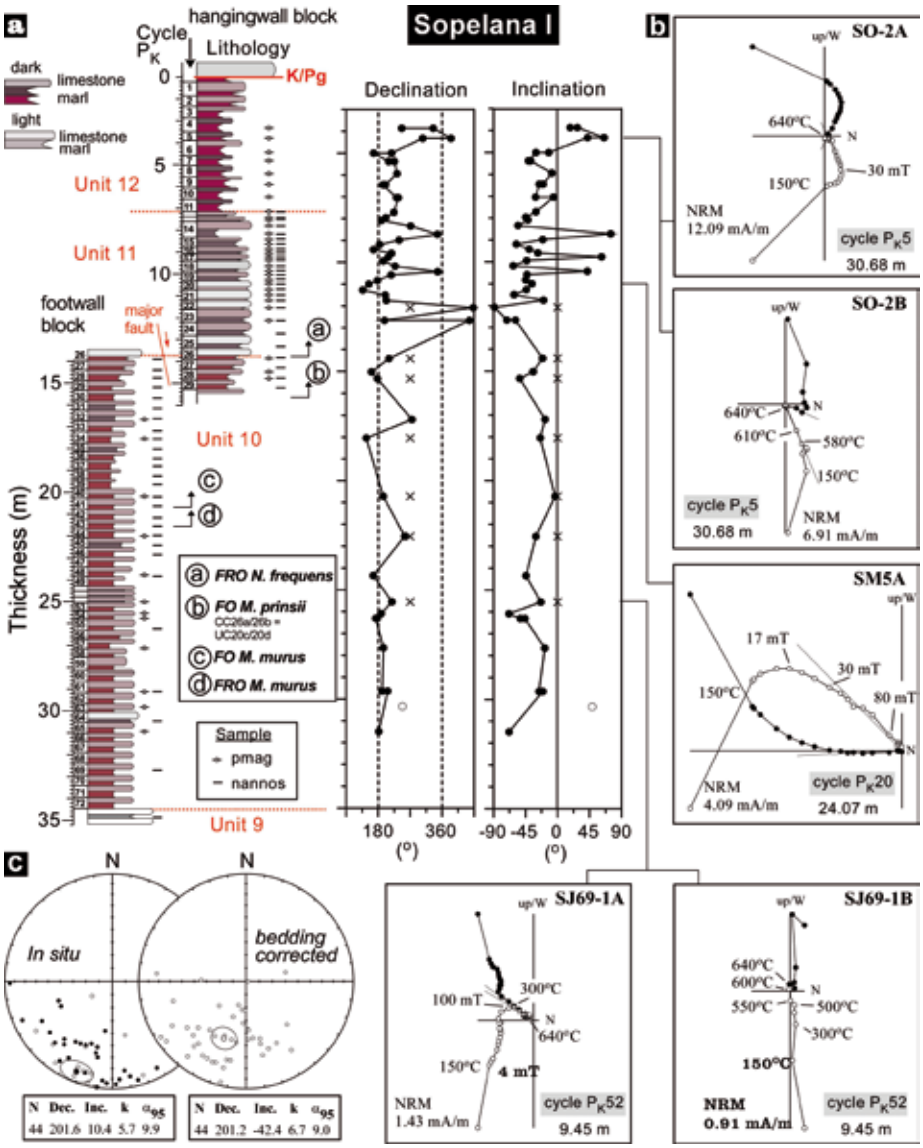

Figure 10. a) Lithological log for Units 10–12 at Sopelana I and declination and inclination computed palaeomagnetic directions on the depth scale through key calcareous nannofossil bioevents; b) some representative orthogonal demagnetization diagrams; and c) stereographic projections of the computed components before (*in situ*) and after bedding correction are shown (open and solid symbols indicate projections onto the upper and lower hemisphere respectively), together with the mean direction and statistics for the secondary reverse directions only.

Figura 10. *a) Columna litológica de las Unidades 10–12 en Sopelana I con las direcciones paleomagnéticas calculadas (declinación e inclinación) y bioeventos de nannofósiles clave; b) algunos diagramas representativos de desmagnetización ortogonal; y c) proyecciones estereográficas de las componentes calculadas antes (*in situ*) y después de la corrección de capa (símbolos vacíos o rellenos indican proyecciones en el hemisferio superior o inferior respectivamente), junto con la dirección media y parámetros estadísticos solo para las direcciones inversas secundarias.*

a latitudinal diachroneity of this datum between the low- and mid-latitude records (Thibault *et al.*, 2010).

The occurrence of *Ceratolithoides kamptneri* is not recorded in the Upper Maastrichtian at Sopelana, thus making it impossible to distinguish the UC 20c subzone (Fig. 4). It does however occur occasionally at some points in many other low-latitude sections (Gardin *et al.*, 2012).

The FO of *Cribrosphaerella daniae* (cycle P_K39, Plate I, 20) is a clearly expressed bioevent following the FO of *M. murus* (cycle P_K41, sample S12-6; Fig. 10). This datum is used as a subzonal marker in the Upper Maastrichtian "tethyan-intermediate" province -North Germany and the Indian Ocean by Burnet (1998). In Sopelana it falls in a position that should correspond to the upper part of C30n. It has, however, been reported close to the C31r/C31n boundary in Hole 1258A (Equatorial Atlantic) by Husson *et al.* (2011). This provides some concern about the isochrony of the datum and therefore its biostratigraphic potential needs to be better assessed.

The FO of *Micula prinsii* in Sopelana (sample SOP-29 in cycle P_K29, Plate I, 14-16; Fig. 10) is recorded relatively low in the succession as this biovent has usually been placed close to the C30n/C29r boundary (*cf.* Herbert *et al.*, 1995; Westerhold *et al.*, 2008). It is a primary biostratigraphic marker for the uppermost part of the Maastrichtian, identifying subzones UC 20d^{TP} and CC 26b in low-latitude sites (Fig. 4), where it is usually reported near the base of C29r. Nevertheless, some recent studies have recorded it at the top of C30n (Self-Trail, 2001; J. Lees, unpublished data). At Sopelana, the FO of *Micula prinsii* is a distinct unambiguous biohorizon the record of which may have been favoured by the predominantly marly litholo-

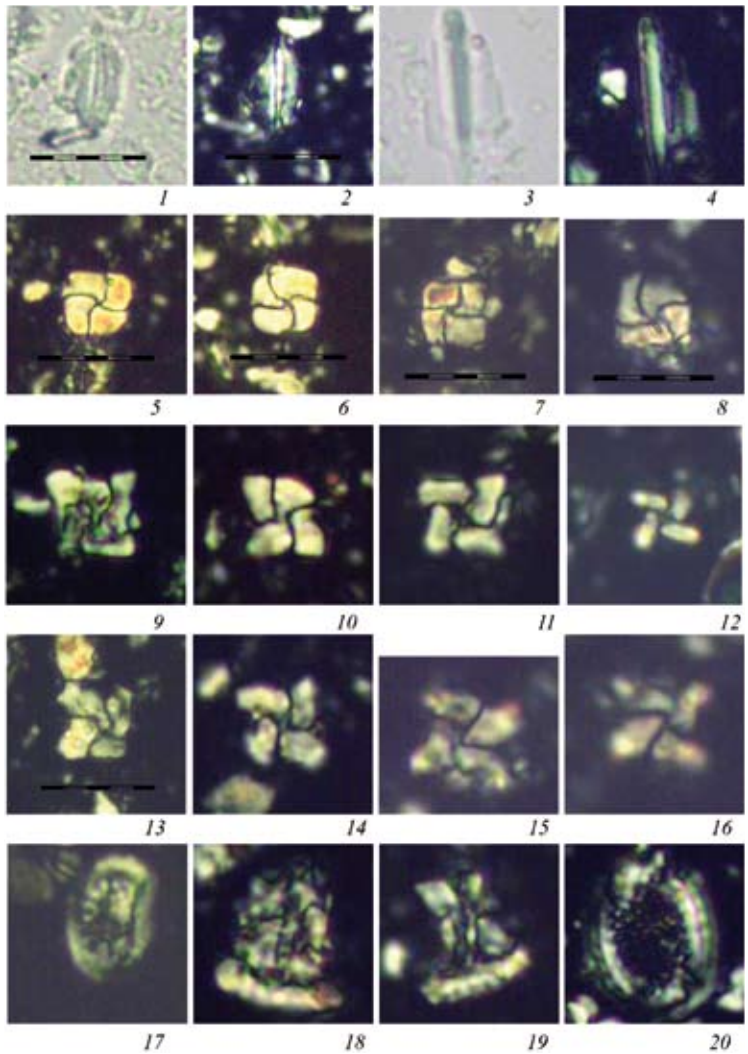

Plate I. Main calcareous nannofossil markers from the Upper Maastrichtian of the Sopelana I section. 1-2 - *Lithraphidites quadratus,* sample B-SO-H. 3-4 - *Lithraphidites quadratus*, sample SM 7. 3 - NL, 4 - XPL. 5 - 6. *Micula praemurus,* sample B-SO-I. 7 - *Micula praemurus,* sample B-SO-F. 8 - *Micula swastica,* transitional form to *M. murus,* sample B-SO-I. 9 - *Micula murus,* sample SM 5. 10 - *Micula murus,* sample SM 7. 11 - *Micula murus,* sample SM 6. 12 - *Micula murus,* FO in sample S12-6. 13 - *Micula prinsii,* sample C-SO-16. 14 - *Micula prinsii,* sample SM 15. 15-16 - *Micula prinsii*, sample SM 3. 17 - *Nephrolithus frequens,* sample C-SO-14. 18 - *Prediscosphaera majungae*, sample SM 9. 19 - *Prediscosphaera majungae*, sample SM 12. 20 - *Cribrosphaera daniae*, sample SM 4. Scale bar 10 μm.

Plate I. *Principales marcadores de nanofósiles calcáreos del Maastrichtiense superior de la sección Sopelana I. 1-2* - Lithraphidites quadratus, *muestra B-SO-H. 3-4* - Lithraphidites quadratus*, muestra SM 7. 3 - NL, 4 - XPL. 5 - 6.* Micula praemurus, *muestra B-SO-I. 7* - Micula praemurus, *muestra B-SO-F. 8* - Micula swastica, *froma transicional a* M. murus, *muestra B-SO-I. 9* - Micula murus, *muestra SM 5. 10* - Micula murus, *muestra SM 7. 11* - Micula murus, *muestra SM 6. 12* - Micula murus, *FO in muestra S12-6. 13* - Micula prinsii, *muestra C-SO-16. 14* - Micula prinsii, *muestra SM 15. 15-16* - Micula prinsii*, muestra SM 3. 17* - Nephrolithus frequens, *muestra C-SO-14. 18* - Prediscosphaera majungae*, muestra SM 9. 19* - Prediscosphaera majungae*, muestra SM 12. 20* - Cribrosphaera daniae*, muestra SM 4. Escala 10 μm.*

Nannofossil bio-events	Stratigraphic interval	Sample	Precession cycle code
FRO *Nephrolithus frequens*	Upper Maastrichtian	C-SO-14	P_K26
FO *Micula prinsii*	Upper Maastrichtian	SO-29	P_K29
FRO *Micula prinsii*	Upper Maastrichtian	SO-30	P_K30
FO *Cribrosphaerella daniae*	Upper Maastrichtian	S12-8	P_K39
FO *Micula murus*	Upper Maastrichtian	S12-6	P_K41
FRO *Micula murus*	Upper Maastrichtian	S12-4	P_K43
FRO *Cribrosphaerella daniae*	Upper Maastrichtian	S12-4	P_K43
FO *Micula praemurus*	Upper Maastrichtian	B-SO-I	P_E1
FO *Prediscosphaera majungae*	Upper Maastrichtian	B-SO-H	P_E2
FO *Lithraphidites charactozorro*	Upper Maastrichtian	B-SO-H	P_E2
FRO *Micula praemurus*	Upper Maastrichtian	B-SO-G	P_E4-5
FO *Lithraphidites quadratus*	Upper Maastrichtian	B-SO-F	P_E6
Local acme of *Braarudosphaera bigelowii*	Upper Maastrichtian	B-SO-C	P_E8
FRO *Lithraphidites quadratus*	Upper Maastrichtian	B-SO-B	P_E9
FO *Lithraphidites praequadratus*	Lower Maastrichtian	SM101	P_E18
FRO *Lithraphidites praequadratus*	Lower Maastrichtian	SM100	P_E19

Table 1. Position of calcareous nannofossil bioevents in the Sopelana I section with respect to the identified precession cycle (P_Kn, precession cycle counting from the K/Pg boundary; P_En, precession counting cycle from the top of Unit 6 or "top Escalón")

Tabla 1. *Posición de los bioeventos de nanofósiles calcáreos en la sección de Sopelana I en relación con el ciclo de precesión en que se identifican (P_Kn, ciclo de precesión contando desde el límite K/Pg; P_En, ciclos de precesión contando desde la parte superior de la Unidad 6 o "top Escalón ")*

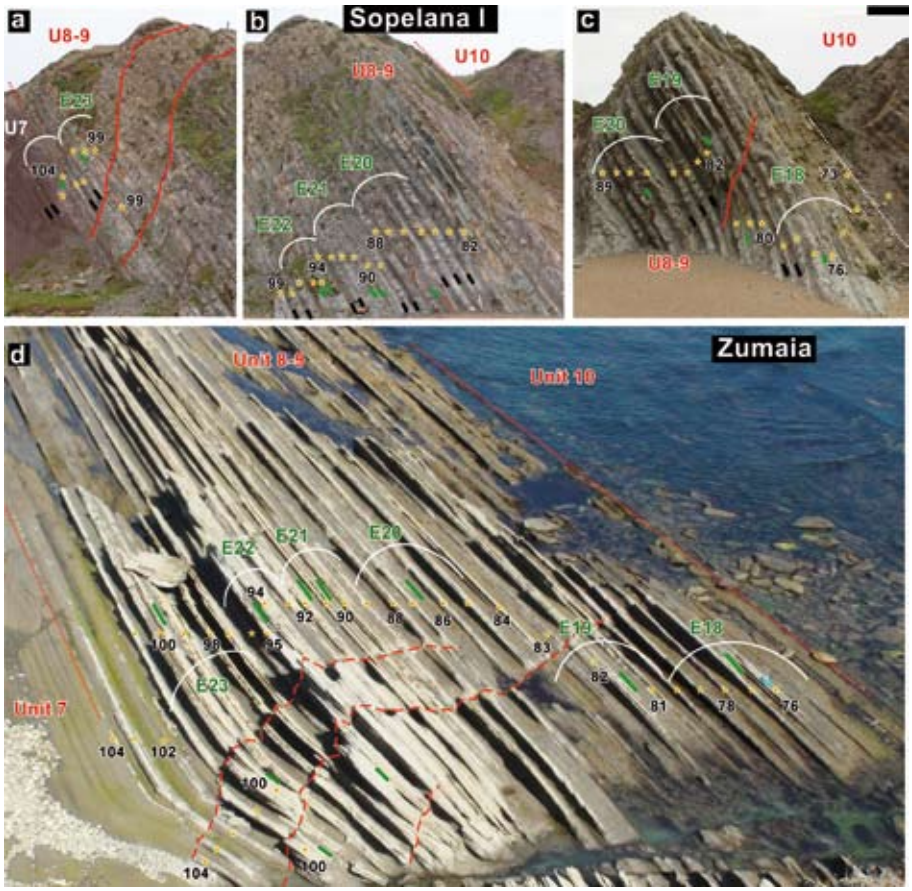

Figure 11. Field photographs of Units 8–9 from cliffs at Sopelana I (a-c) and the Zumaia wave-cut platform at low tide seen from the cliff (d). The numbering of the precession couplets P_K73–P_K104 and the eccentricity-related bundles E18–E23 descends from the overlying Units 11–12. Relatively pronounced marly layers are marked in black whereas less contrasted marly interlayers are marked in green (see text for discussion).

Figura 11. *Fotografías de campo de las Unidades 8–9 de los acantilados en Sopelana I (a-c) y rasa mareal de Zumaia en baja marea desde el acantilado (d). La numeración de los pares de precesión P_K73–P_K104 y los paquetes de excentricidad E18–E23 desciende desde las Unidades 11–12 sobreyacentes. Capas de marga relativamente marcadas están señaladas en negro, mientras que capas de marga menos contrastadas están marcadas en verde (véase el texto para la discusión).*

gies deposited in a setting devoid of turbidites. In this study the calibration of this datum at about 609 ky below the K/Pg boundary, within chron C30n, may imply either diachrony or the erroneous calibration of the existing biostratigraphic data. For example, at Zumaia, situated just some 70 km from Sopelana, it has been documented close to the K/Pg boundary in C29r (Lees in Pérez-Rodríguez *et al.*, 2012) (Fig. 2), although the reported poor preservation there may have some significance. Furthermore, Thibault *et al.* (2012), in his integrated study on ODP Hole 762C from the Indian Ocean, have calibrated the bioevent at 390±70 ky below the K/Pg boundary. Nevertheless, we note that this bioevent has already been shifted to an older age in the GTS2012 time scale (Gradstein *et al.*, 2012) (Fig. 4), although no explanation is provided.

The First Rare Occurrence (FRO) of *Nephrolithus frequens* (sample C-SO-14 in cycle P_K26, Plate I, 20) is observed in the uppermost part of the succession (Fig. 10). It has been used to define the base of CC 26a (Fig. 4), but then it has been proved to be time-transgressive toward the equator in high southern latitudes (Pospichal *et al.*, 1992). In Sopelana its occurrence is rare but consistent throughout the uppermost part of the Maastrichtian UC20d^{TP} zone.

Units 9–7

Determining the cyclic stacking pattern for Units 9–8 and counting precession cycle (i.e. marl-limestone couplets) and eccentricity-related bundles is relatively straightforward. The field photographs from Figure 11 illustrate this interval both at Zumaia and Sopelana I. A total of 32 precession-related couplets can be recognised (cycles P_K73 to P_K104) comprising 6 eccentricity-related cycles, which we have denominated E18 to E23 (following the 17 eccentricity cycles from Units 12–10). These 100-ky eccentricity cycles are made evident by a series of two or three consecutive basic couplets containing relatively well developed marly layers that must correlate with eccentricity maxima, while the eccentricity minima are marked by one or two low-amplitude couplets containing less developed marly interlayers, which are clearer in the images at Sopelana (Figs. 11a-c).

The relatively marly reddish Unit 7 is better exposed at Zumaia (Fig. 12) whereas it appears tectonized and possibly truncated/reduced at Sopelana (Fig. 3). A close examination of Unit 7 at Zumaia under good lighting conditions reveals the same stacking pattern observed in the overlying units, particularly

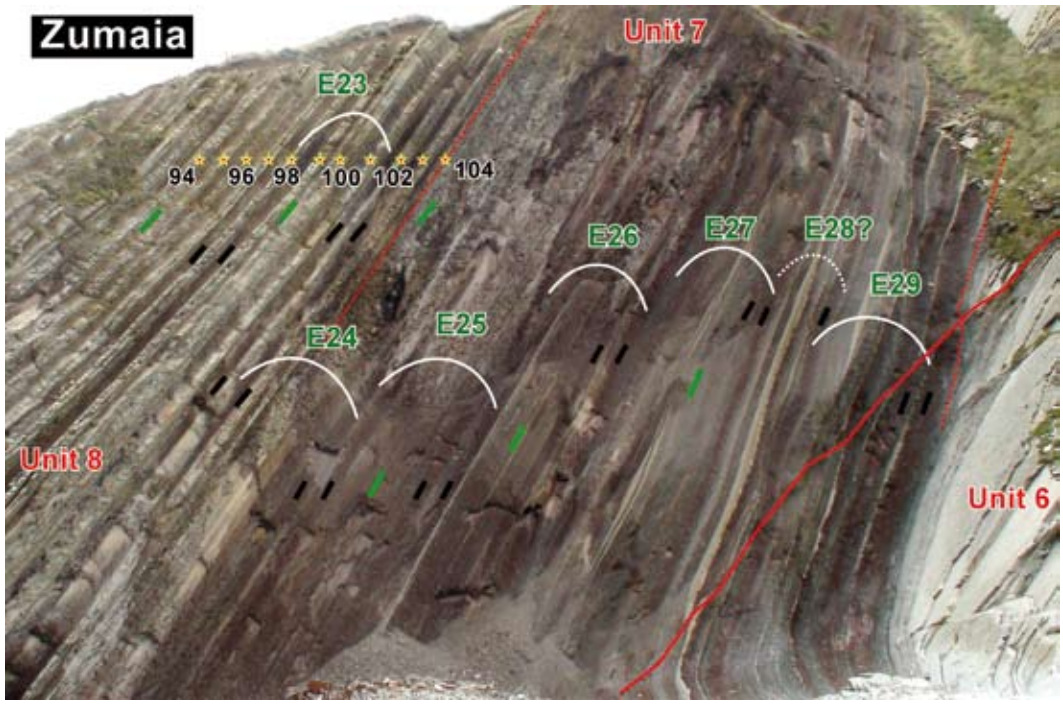

Figure 12. Field photograph of Unit 7 at Zumaia, on which eccentricity cycles are numbered (E24–E29).
Figura 12. *Fotografía de campo de la Unidad 7 en Zumaia, en la que se han numerado los ciclos de excentricidad (E24–E29).*

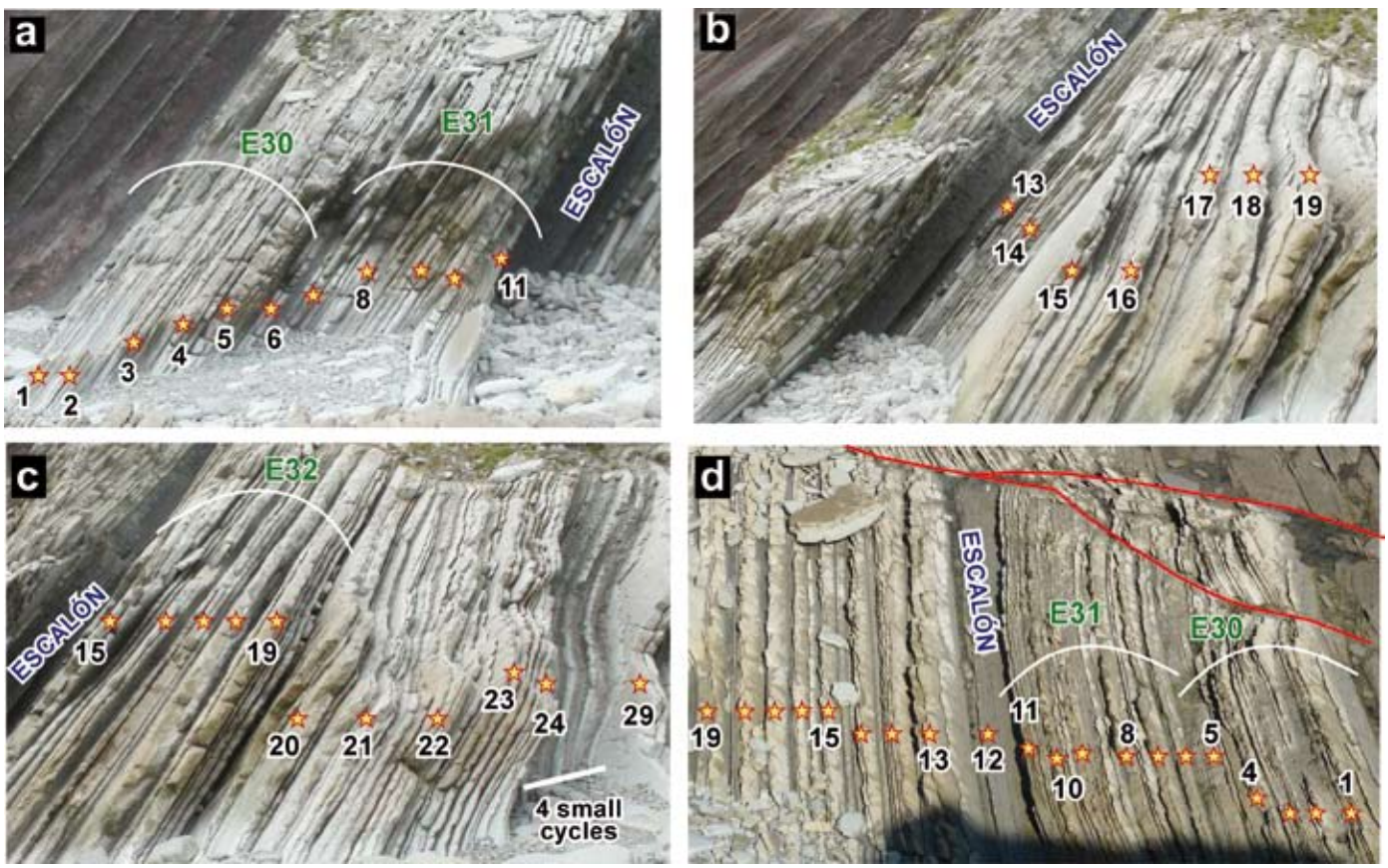

Figure 13. Field photographs of Unit 6 showing the conspicuous marly Escalón at the sea-cliff (a-c) and Zumaia wave-cut platform (d) exposures. Individual couplets are numbered from the top of this unit downward.
Figura 13. *Fotografías de campo de la Unidad 6, mostrando el llamativo Escalón margoso visible en el acantilado (a-c) y en afloramientos de la rasa mareal (d) de Zumaia. Los pares están numerados desde la parte superior de la unidad hacia abajo.*

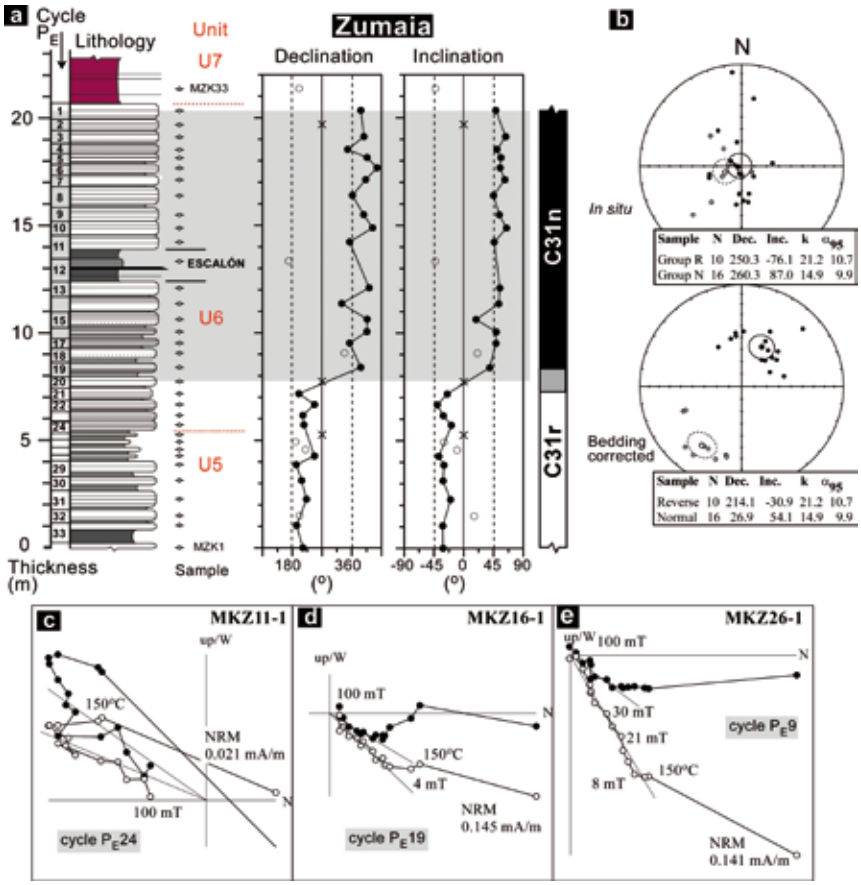

Figure 14. a) Lithological log for Unit 6 at Zumaia and declination and inclination computed palaeomagnetic directions on the depth scale; b) stereographic projections of the computed components before (*in situ*) and after bedding correction are shown, together with the mean direction and statistics for the normal and reverse directions; and c-e) some representative orthogonal demagnetization diagrams.

Figura 14. *a) Columna litológica de la Unidad 6 en Zumaia con las direcciones paleomagnéticas calculadas (declinación e inclinación); b) proyecciones estereográficas de las componentes calculadas antes (*in situ*) y después de corrección de capa junto con la dirección media y estadísticas para las direcciones normales e inversas; y c-e) diagramas representativos de desmagnetización ortogonal.*

the eccentricity-related bundles (Fig. 12). As lithological couplets are difficult to distinguish within some intervals we have not counted them in this unit and only take into account the eccentricity-related bundles. The E26 cycle is not clear because several relatively thicker conspicuous turbiditic layers are interbedded within this lower part of Unit 7.

Unit 6

Unit 6 is characterized at Zumaia as a ~15-metre-thick carbonate-rich package with a characteristic 1.2-metre-thick marly interval (including a couple of thin turbidites) in the middle that is nick-named "Escalón" (Fig. 13). The marly beds of the precession-related couplets throughout this interval are poorly developed and several partitions and thin to very thin turbidites make distinguishing cyclicity a demanding task. A combination of observations on the sea-cliff wall and the wave-cut platform under different lighting conditions allowed us to discern a total of 24 precession-related couplets and 4-5 eccentricity-related bundles of 4–6 couplets from the top of this unit down to four very characteristic, relatively thin, small marly cycles (cycles 25–28 in Fig. 13). Because the precession cycles are somewhat blurred in Unit 7, counting of the precession-related couplets for Unit 6 re-starts at the top of Unit 7 and are named P_E1 to P_E24. Unit 6 has been targeted to locate precisely the chron C31r/C30n reversal (Fig. 14). Magnetic intensity in these light-grey limestones is relatively low (usually below 0.1 mA/m) but demagnetization of the data is of good quality for most of the samples studied and a clear magnetostratigraphy could be established, as inferred in Pérez-Rodríguez *et al.* (2012), which we can now place in a satisfactory cyclostratigraphic framework. The C31r/C31n is placed at precession cycle $P_E20\pm1$ at the top of Unit 6 at Zumaia, which is discussed further below.

The succession in the Sopelana I section is devoid of turbidites but some structural complications and outcrop conditions make it somewhat difficult to recognise all the cycles and details at first glance. Nevertheless, taking the four characteristic small precession cycles that are clearly visible up in the cliff (Fig. 15a and c) cycles P_E13–P_E24 can be discerned in the top outcrop of the cliff despite the fact that some small faults and intrastratal sliding and folding disrupt the succession a little. Cycles P_E13–P_E21 crop out again at the beach on another block separated by a fault below

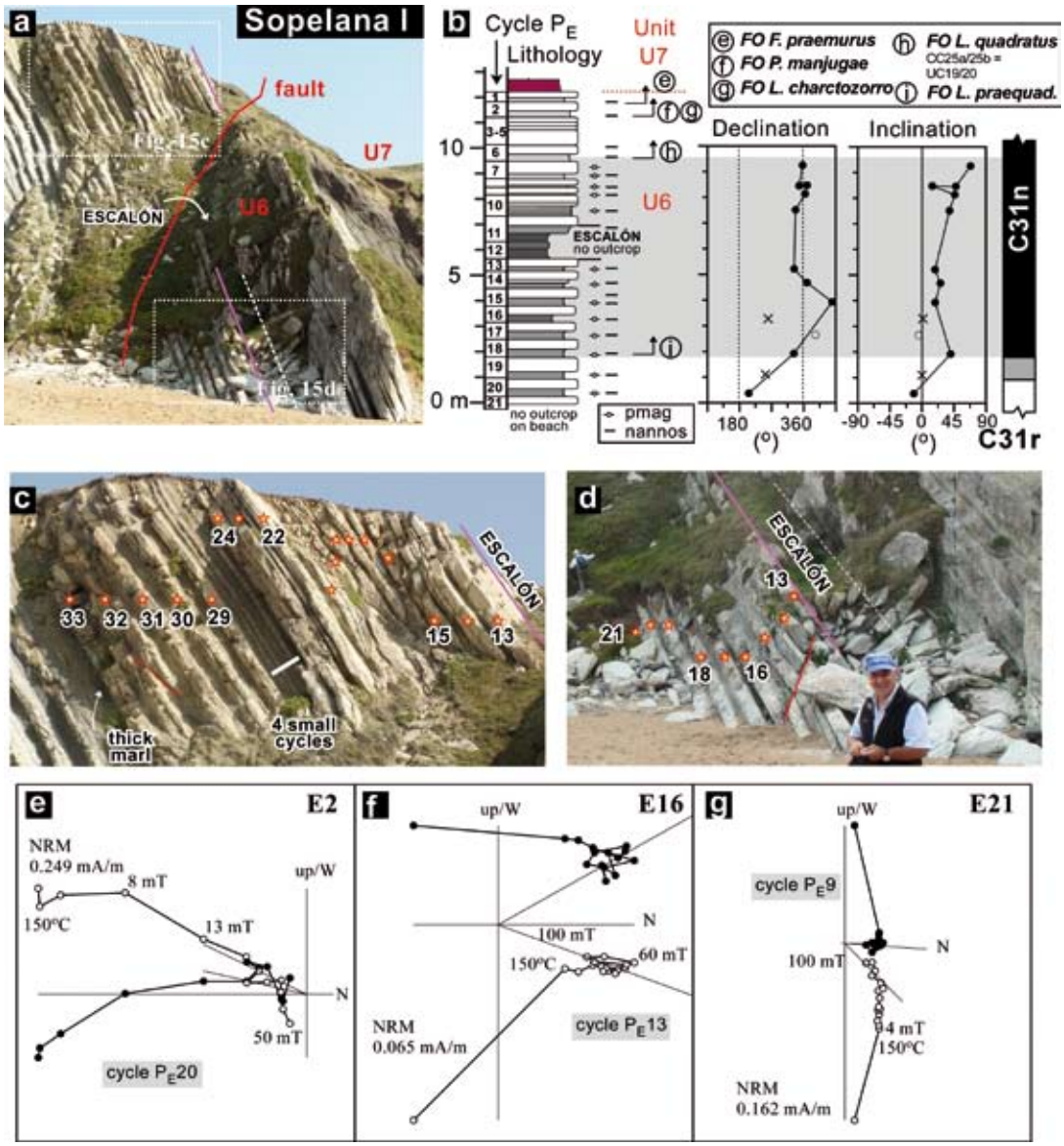

Figure 15. Field photographs (a, c-d) and lithological log (b) for Unit 6 at Sopelana I and declination and inclination computed palaeomagnetic directions on the depth scale through key calcareous nannofossil bioevents, e-g) some representative orthogonal demagnetization diagrams.

Figura 15. *Fotografías de campo (a, c-d) y columna litológica (b) de la unidad 6 en Sopelana I con las direcciones paleomagnéticas calculadas (declinación e inclinación) y bioeventos de nannofósiles clave, c-e-g) diagramas representativos de desmagnetización ortogonal.*

the poorly exposed Escalón (Fig. 15d). Cycles P_E1–P_E11 above the Escalón outcrop on the same block at the beach although some of the cycles are difficult to recognise due to the predominantly carbonate nature of the interval and to some minor disruptions and partitions. Palaeomagnetic sampling through this interval (Fig. 15b) indicates that the C31r/C31n chron boundary must be located between the marly layer of cycle P_E20 and the marly layer of cycle P_E18 (the sample from cycle P_E19 did not provide any interpretable results).

The survey of calcareous nannofossils within this interval indicated the FO of several taxa (see Table 1 for full details). The FO of *Lithraphidites quadratus* (Plate I, 1–4), an important low-latitude biohorizon, is recorded in cycle P_E6 at the top of the unit and cycles P_E12–P_E13 (252–273 ka) above the base of chron C31n. Its position at Sopelana is consistent with the previously reported position in the Umbria-Marche pelagic sections (Gardin *et al.*, 2012) and at Zumaia (Lees in Pérez-Rodríguez *et al.*, 2012). Some previous researchers have considered this biohorizon to be potential marker for the placement of the lower-upper Maastrichtian boundary (Paul and Lamolda, 2007). The species is reported to have wide geographic distribution

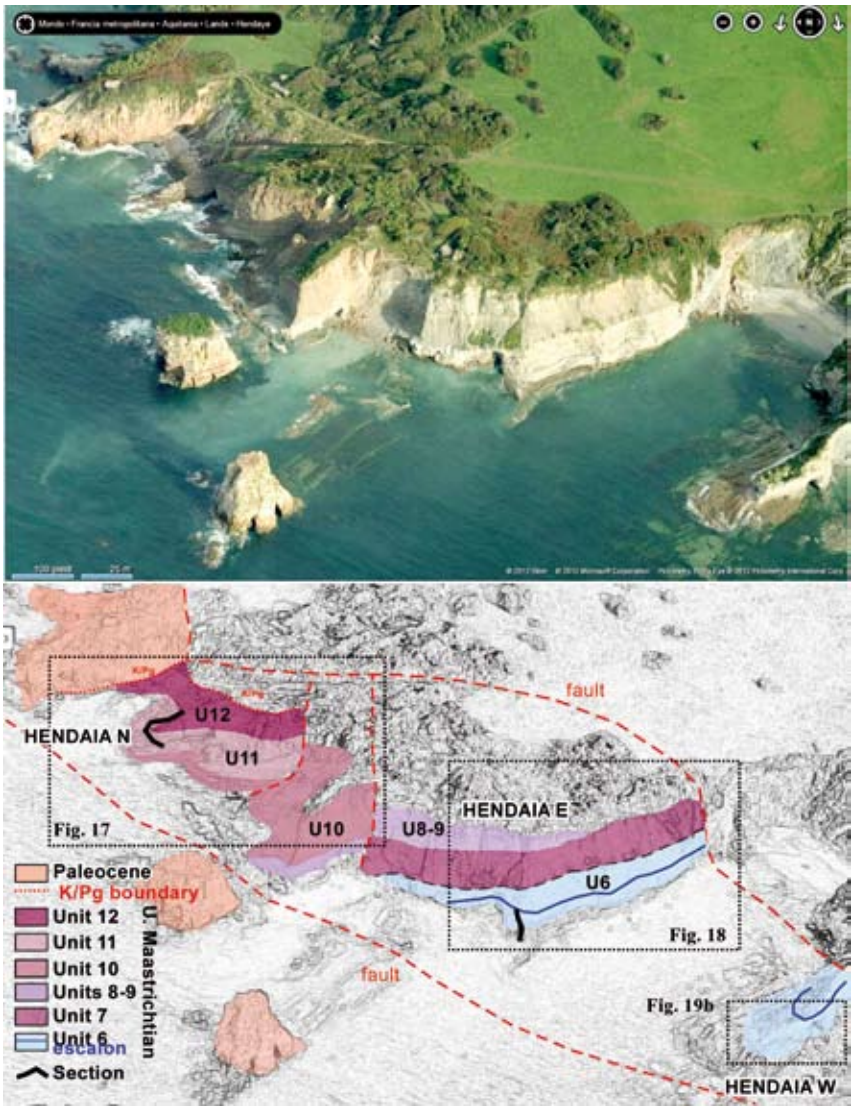

Figure 16. Aerial view of the Pointe Sainte-Anne near Hendaia (from BingMaps) and a sketch showing the main faults and blocks and the classical lithological Units U6–U12 of Wiedmann (1988). The sections studied and the locations of other figures are indicated.

Figura 16*. Vista aérea de la Pointe Sainte-Anne, cerca de Hendaia (de BingMaps) y un dibujo que muestra las principales fallas y bloques y las unidades litológicas clásicas U6–U12 de Wiedmann (1988). Se indican las secciones estudiadas y la ubicación de otras figuras.*

in low-latitude sections and thus can be used as a reliable correlation biohorizon there.

The Hendaia section

It has been seen above that despite some lithological differences between the Zumaia and Sopelana I sections (i.e. lack of turbidites in the second) the previously defined lithological Units 6 to 12 and marl and limestones beds can be correlated bed-by-bed between these two sections some 70 km apart. The origin of these main differences is probably related to the particular depositional setting of each section within the deep-water trough. In order to explore further and substantiate the findings at Zumaia-Sopelana I, additional research has been undertaken in other Basque sections. Here, we only provide the results from the less well known Hendaia locality at the Pointe Sainte-Anne because it provides some better clues for the cyclic details of Unit 6 and the position of the C31r/C31n reversal. Also, an attempt to document the location of the C30n/C29r chron reversal has been undertaken.

The Upper Maastrichtian succession crops out in a series of spectacular coastal-cliffs around the Pointe Sainte-Anne near Hendaia, which are difficult to access and only partly accessible at low tide (Fig. 16). Although bedding is subhorizontal or gently dipping, the area is cross-cut with several small-scale and also some more important faults and peculiar contacts. Nevertheless, the general lithostratigraphic units can be recognised (see sketch in Fig. 16). The upper part of the Maastrichtian at the contact between Units 11–12 has been studied at the northern end of the cape (Hendaia N section) (Fig. 17). Palaeomagnetic measurements in 13 samples from 10 consecutive cycles spanning cycles P_K8–P_K19

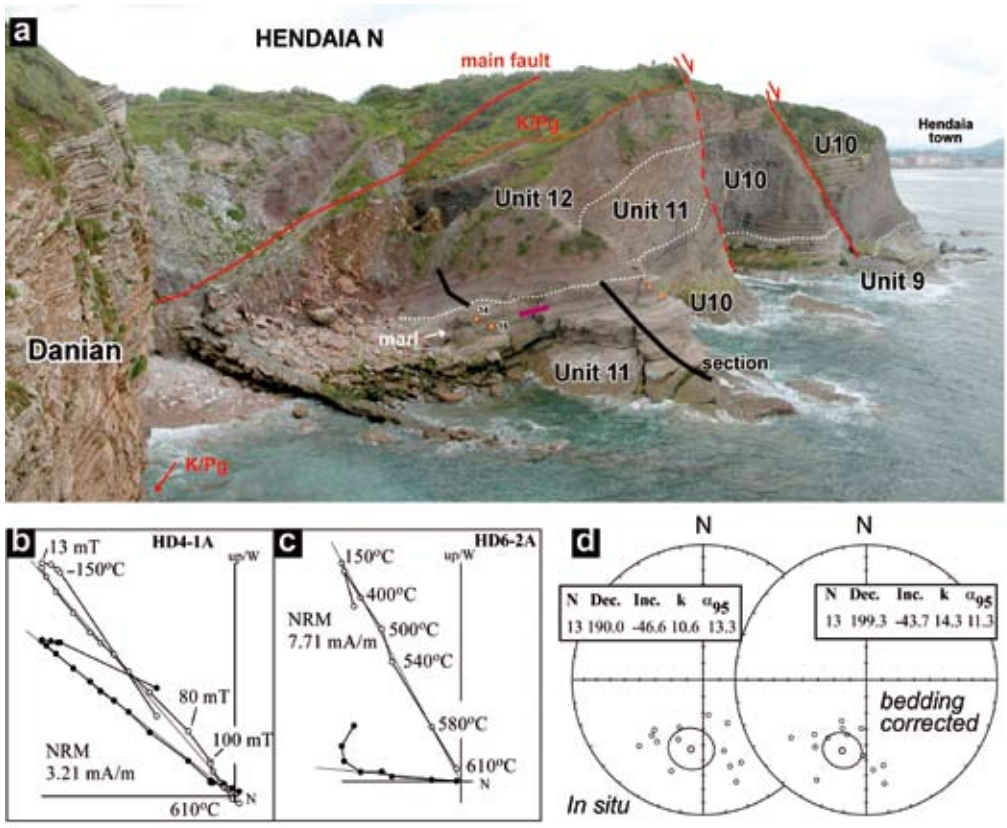

Figure 17. (a) Field photograph of the Hendaia N section with main fault and lithological Units U9–U12 indicated; (b-c) representative orthogonal demagnetization plots; and (d) stereographic projections of the computed components before (*in situ*) and after bedding correction together with the mean direction and statistics for the secondary reverse directions.
Figura 17. *(a) Fotografía de campo de la sección de Hendaia N donde se señalan la falla principal y las Unidades litológicas U9–U12; (b-c) diagramas ortogonales de desmagnetización representativos; y (d) proyecciones estereográficas de las componentes calculadas antes (*in situ*) y después de la corrección de capa junto con la dirección media y parámetros estadísticos para las direcciones inversas secundarias.*

within the expected interval for the C30n/C29r boundary only indicate reverse polarities (Figs. 17b–d), which can be put down to a secondary pervasive overprint in those lithologies, much in the line with the observations made at Zumaia and Sopelana. Consequently, we were unable to locate this chron boundary in any of the sections investigated in the Basque Basin.

Unit 6 was studied in the central area of the Pointe Sainte Anne outcrop, along a section we have named Hendaia E. Within this outcrop Unit 6 is less carbonate than in Zumaia-Sopelana I and outstanding precession cycles are obvious (Fig. 18), with the conspicuous Escalón showing up clearly, especially when a weathered profile is seen (Fig. 18b and Fig. 19a). Magnetostratigraphy through cycles P_E14–P_E23 below the top of the unit confirms and substantiates that the C31r/C31n boundary occurs at cycle P_E20 (8 cycles below the Escalón, Fig. 18c). Figure 19 displays views of Unit 6 at Hendaia E and Hendaia W, which is located not far on the other side of the bay (Fig. 16) and also at Zumaia. Despite the short distance the two Hendaia outcrops display slightly different characteristics, Hendaia E having some reddish colouring through the lower interval, but otherwise all the precession cycles and particularities match bed-by-bed among the three sections. In particular the four small cycles below cycle P_E24, the prominent marl below cycle P_E33 and the two relatively well developed marls in cycles P_E29 and P_E30 are clearly seen (see also this interval at Sopelana I in Fig. 15c).

Discussion

Much controversy has been generated about the absolute age of the K/Pg boundary, which seems to jump as much as 1 My even in the most recent Geological Time Scales. An age of 65 Ma was reported by Berggren *et al.* (1995) whereas 65.5 Ma was adopted in the GTS2004 (Gradstein *et al.*, 2004) without incorporating cyclostratigraphic constraints. Using the first modern astronomical solution, Va03_R7, by Varadi *et al.* (2003) we tuned the K/Pg boundary at Zumaia to an age of

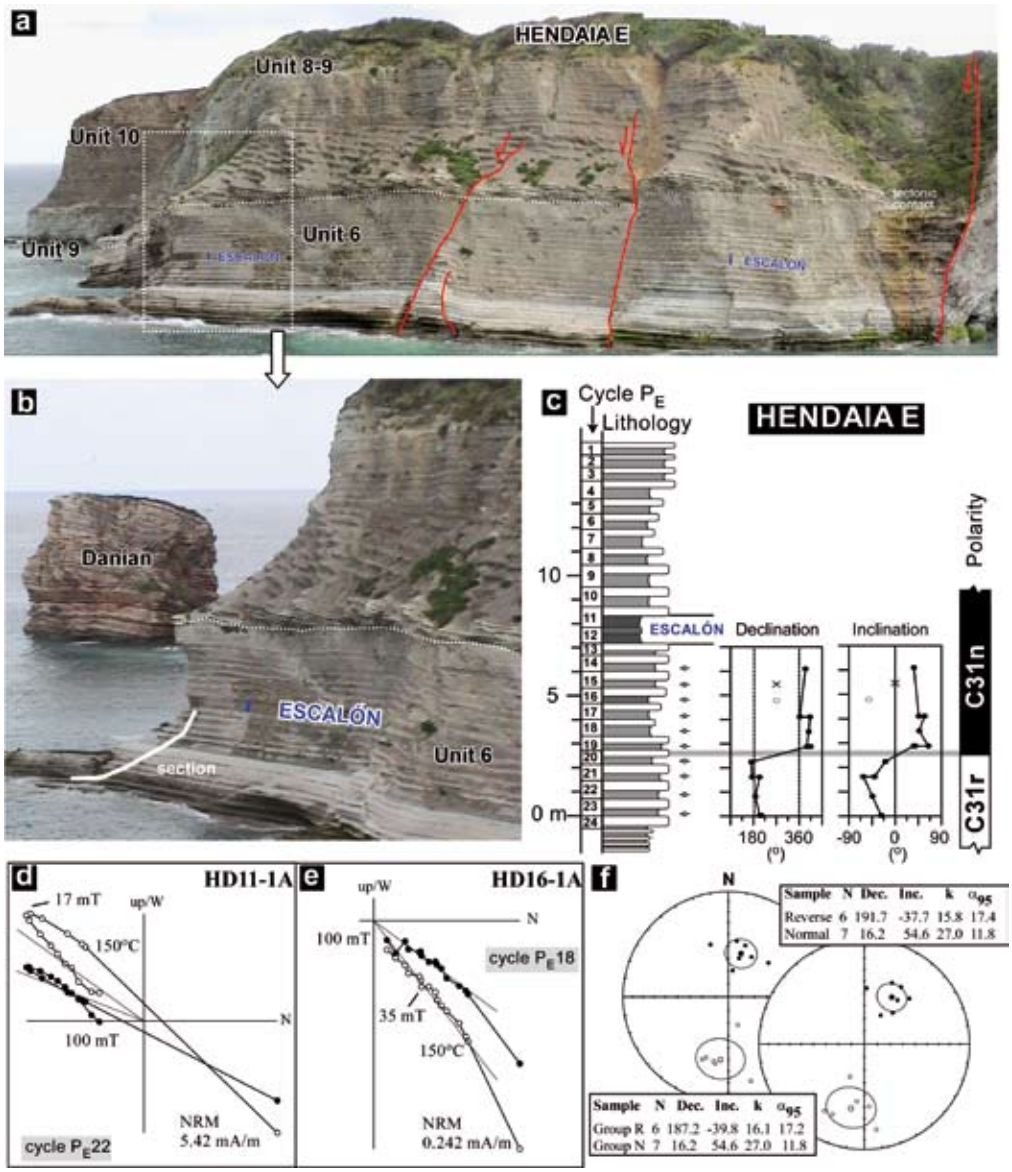

Figure 18. Field photographs (a-b) and lithological log (c) for Unit 6 at Hendaia E and declination and inclination computed palaeomagnetic directions on the depth scale; (d-e) some representative orthogonal demagnetization diagrams; and (f) stereographic projections of the computed components before (*in situ*) and after bedding correction, together with the mean direction and statistics for the normal and reverse directions.

***Figura 18**. Fotografías de campo (a-b) y columna litológica (c) de la Unidad 6 en Hendaia E con las direcciones paleomagnéticas calculadas (declinación e inclinación); (d-e) diagramas de desmagnetización ortogonal representativos; y (f) proyecciones estereográficas de las componentes calculadas antes (*in situ*) y después de la corrección, junto con la dirección media y parámetros estadísticos para las direcciones normales e inversas.*

65.83 Ma (Dinarès-Turell *et al.*, 2003) by using as first anchoring point the expression of a node in the very long eccentricity cycle in the upper part of the Danian, and then tuning consecutive short eccentricity-related bundles and precession cycles down to the K/Pg boundary, which is less accurate than tuning the 405-ky eccentricity cycle for these older ages but still a good metronome. The Palaeocene tuning at Zumaia was revisited by Westerhold *et al.* (2008), Kuiper *et al.* (2008) and Hilgen *et al.* (2010) in the light of a newly available solution (the La2004 solution, Laskar *et al.*, 2004) and basing the tuning on the more stable 405-ky eccentricity cycle and some reinterpretation of cycle identification. Due to uncertainties in the radioisotope monitor standards these authors provided several options by offsetting tuning to consecutive 405-ky cycles, thus attaining different ages for the K/Pg boundary. The favoured tuning option to La2004 in Kuiper *et al.* (2008) and Hilgen *et al.* (2010), following the 405-ky tuning strategy, placed the K/Pg boundary at 65.95 Ma, which is basically the same as in Dinarès-Turell *et al.* (2003) (the difference arising from the interpretation of an additional 100-ky eccentricity cycle in the Zumaia record), an age that was in accord with the authors' new re-evaluation of the Fish Canyon Sanidine (FCS) monitor standard, at 28.20 Ma. The three tuning options for the K/Pg boundary provided in Westerhold *et al.* (2008), 65.28 Ma, 65.68 Ma and 66.08 Ma respectively, have been looked upon both favourably and disfavourably, while the most recent calibration via the earliest Palaeogene, which is independent of the radioisotope ages and uses the La2011 orbital solution (Westerhold

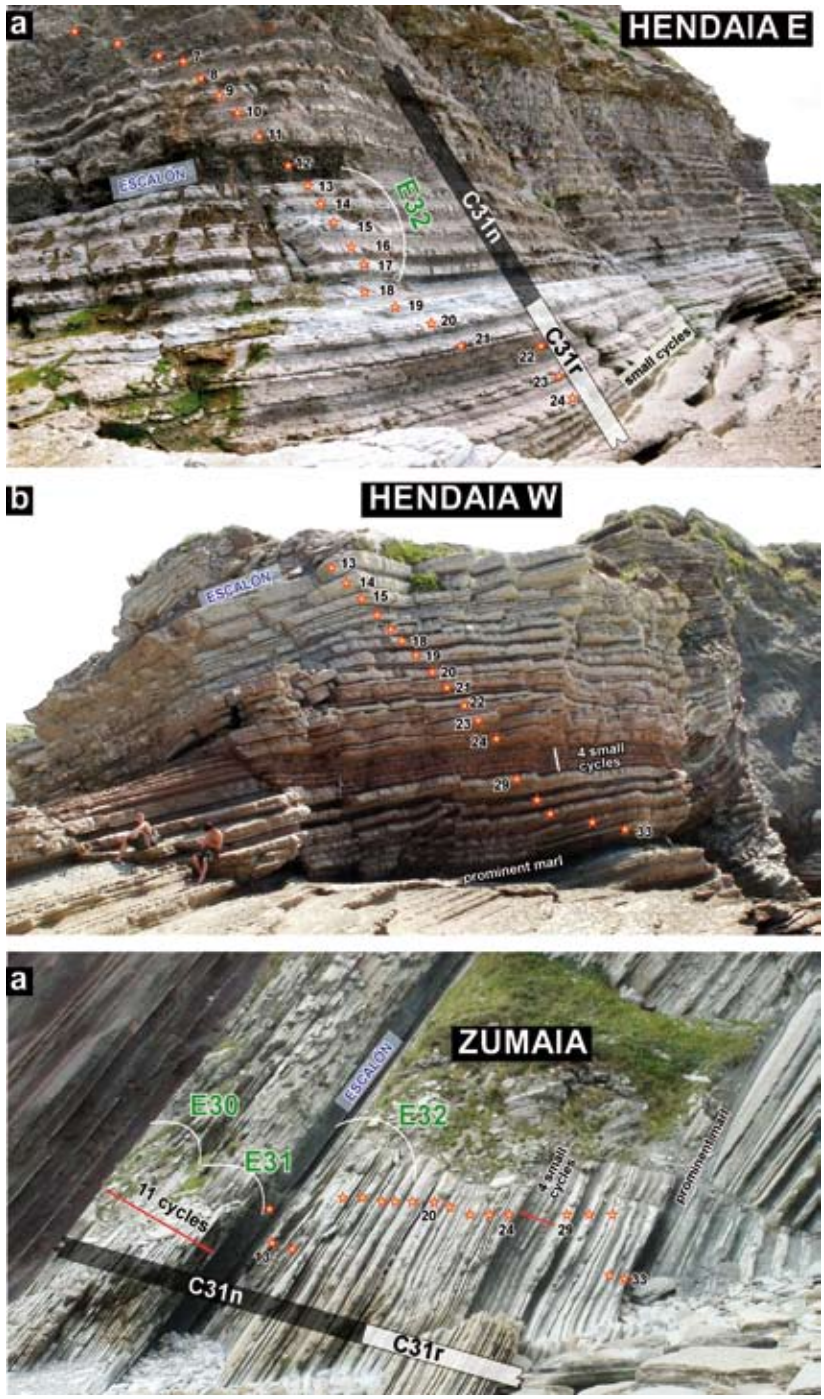

Figure 19. Field photographs of Unit 6 at the Hendaia E (a), Hendaia W (b) and Zumaia (c) sections, showing the numbered precession-related couplets, the recovered magnetostratigraphy and some peculiar features including the Escalón, four consecutive small cycles and a prominent marl bed below cycle 33 (Fig. 15c for the same features at Sopelana I).

Figura 19. *Fotografías de campo de la Unidad 6 en las secciones de Hendaia E (a), Hendaia W (b) y Zumaia (c), mostrando los pares de precesión numerados, la magnetoestratigrafía medida y algunas características peculiares como el Escalón, cuatro ciclos pequeños consecutivos y un nivel de marga prominente bajo el ciclo ciclo 33 (ver Fig. 15C para las mismas particularidades en Sopelana I).*

et al., 2012), controversially indirectly recalibrates the FCS at 27.89 Ma and puts the K/Pg at 65 250 Ma, which is close to their earliest option 1. Other inferences on tuned Maastrichtian deep-sea records by Husson *et al*. (2011) that seem to have been incorporated into the last Geological Time Scale (Gradstein *et al*., 2012) favour the estimate of the K/Pg boundary at about 66 Ma, close to a 405-ky minimum around that age. It is out of the scope in this paper to further scrutinise the Palaeocene orbital tuning and absolute age of the K/Pg boundary, and for practical reasons we have adopted the age of ~66 Ma for the K/Pg and used the La2010d orbital solution as a template for our Upper Maastrichtian framework whilst acknowledging that this solution can only be taken as tentative and only valid for the 405-ky eccentricity cycle.

A direct cycle counting and bandpass filtering output is the basis of our cyclostratigraphic framework for

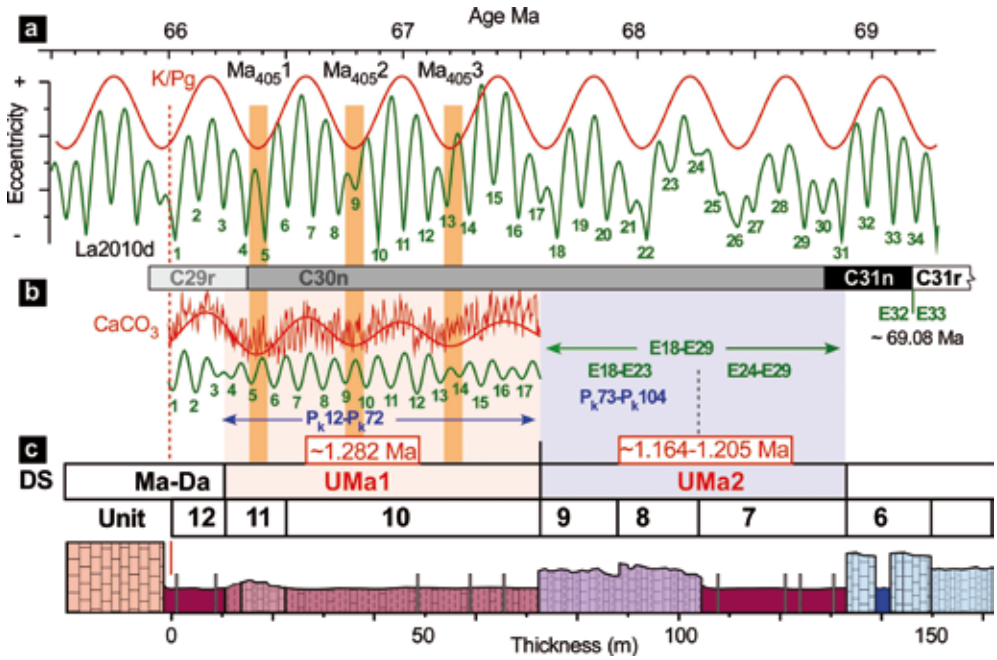

Figure 20. (a) Eccentricity orbital solution La2010d (Laskar *et al.*, 2011b) with the extracted 405-ky long eccentricity for the Late Maastrichtian interval. The K/Pg boundary is located at about 66 Ma, close to a long eccentricity minimum; (c) Zumaia inferred and measured magnetostratigraphy, carbonate record for Units 10–12 (Ten Kate and Sprenger, 1993), and derived filters to extract the short (E green) and long (M_{400} red) eccentricity cycles that are numbered at their minima. The number of the precession-related cycles (P_K cycles in blue) and short eccentricity cycles (E cycles in green) for some intervals is indicated. (c) Synthetic lithological log with the lithostratigraphic units and depositional sequences (DS) (see text for discussion).

Figura 20. *(a) Solución orbital de la excentricidad La2010d (Laskar* et al.*, 2011b) con la excentricidad larga de 405-ka extraída para el intervalo Maastrichtiense final. El límite K/Pg está situado a unos 66 Ma, cerca de un mínimo de la excentricidad larga; (c) magnetostratigrafía medida y deducida en Zumaia y registro de carbonato para las Unidades 10–12 (Ten Kate y Sprenger, 1993) y filtros derivados para extraer los ciclos de la excentricidad corta (E verde) y larga (M_{400} rojo) que se numeran en sus mínimos. Está indicado el número de los ciclos de precesión (ciclos P_K en azul) y ciclos de excentricidad corta (E ciclos en verde) para algunos intervalos. (c) columna litológica sintética con las unidades litoestratigráficas y secuencias deposicionales (DS) (véase el texto para la discusión).*

the Upper Maastrichtian in the Basque Basin. Figure 20 displays the salient features of this framework, taking Zumaia as the master section. Bearing in mind the position of the K/Pg boundary as outlined above, the Zumaia record can be tuned to the La2010d orbital solution (Laskar *et al.*, 2011b) in accordance with the 405-ky cycle. Therefore, the three consecutive eccentricity-related cycles, $Ma_{405}1$ to $Ma_{405}3$, can be tuned to successive eccentricity minima of that cycle in the orbital solution. Note that we code the eccentricity minima rather than the maxima, as has been the practice of other authors (*cf.* Westerhold *et al*, 2008, Husson *et al.*, 2011, Thibault *et al.*, 2012), because we feel it more useful and practical in those land-based sections where carbonate-rich or low-amplitude intervals are usually prominent and stand out in the field. For lithological Units 8-9 we provide direct counting of individual precession-related couplets or P_k cycles and 100-ky eccentricity cycles (Fig. 20b). For marly Unit 7, for which individual precession cycles are somewhat blurred, we only provide eccentricity counting. Consequently, counting the precession-related couplets for the underlying Unit 6 starts at the top of this unit, referred to as "top Escalón" (P_E cycles). The exact genetic nature and significance of the two conspicuous marly couplets constituting the Escalón remains unclear. We put them down to an eccentricity maximum but the possibility that may represent a local/regional tectonically driven sea-level or climatic event deserves further attention. Under this cyclostratigraphic scheme, chron C31r/C31n occurs slightly below the eccentricity maximum between cycles E32-E33 (20 precession cycles below the top of the unit at P_E20), (Fig. 20 and discussion above). In the Maastrichtian astronomical calibration of Husson *et al.* (2011), ODP Site 525A in the South Atlantic is chosen to calibrate this reversal boundary. In their option 2, which takes the K/Pg boundary to occur at about 66 Ma, the C31r/C30n boundary is calibrated at 69.22±0.07 Ma (i.e. 3.22 Ma older than the K/Pg boundary), and close to their eccentricity maximum labelled 32, which would correspond exactly to the maximum between our E32-E33 cycles. This is fairly consistent with our calculation but it is not clear how Husson *et al.* (2011) reached the figure of 3.22 My reported in their Table 3 for the position of C31r/C31n rela-

tive to the K/Pg boundary. It looks as though they have added the duration of the Maastrichtian part of chron C29r (0.3 My), C30n (1.9 My), C30r (~0.12 My) and C31n (~0.9 My), which combine data from sites 1267B and 525A, as they report in Table 1, although it still remains unclear which orbital cycles they base their counting and duration estimates upon. Anyway, we could take the absolute age of the eccentricity maximum between cycles E32 and E33 in the La2010d solution (69027 Ma) and add two precession cycles to account for the inferred position at cycle P_E20, just below the eccentricity maximum, to reach a figure of ~69.08 Ma or ~3.08 My from the K/Pg boundary (Fig. 20).

Furthermore, the cyclostratigraphic framework allows us to estimate the duration of the 3rd-order depositional sequences, which have been interpreted as controlled by sea-level variations (see Introduction). It is obvious that a rate of close to 1.2 My seems to be valid for the two late Maastrichtian depositional sequences UMa-1 and UMa-2 (Fig. 20). The duration of 1.28 My estimated for UMa-1 comes directly from counting precession-related couplets for Units 10-11 (61 cycles, P_K12–P_K72) and taking an average duration of ~21 ka (Fig. 20). The estimate of 1 164–1 205 Ma for UMa-2 derives from the use of two slightly different calculations. One (1 205 Ma) relies on the addition of 32 precession cycles plus 5.5 short eccentricity cycles with an estimated duration of 97 ky (Maastrichtian mean duration calculated from the La2010d solution). The second (1 164 Ma) is based on an estimation of 12 short eccentricity cycles for the interval comprising Units 7–9 (Fig. 20). We also note that the Ma-Da depositional sequence fits the same pattern and duration as it comprises 8 (possibly 9) eccentricity cycles in the Danian (*cf.* Dinarès-Turell *et al.*, 2003) and 2-3 in the Maastrichtian part. The sea-level drop at the base of UMa-2 close to the Lower/Upper Maastrichtian boundary may be a causal factor in the mid-Maastrichtian extinction which affected the Inoceramidae, rudist bivalves and other molluscs, as well as a sharp decline in the ammonites (*cf.* Ward *et al.*, 1991; Ward and Kennedy, 1993). Stable isotope data from inoceramid shells throughout the latest Lower Maastrichtian in the Basque Basin, which have undergone the diagenetic effects of burial processes, still preserve the trends of palaeo-environmental signals (Gómez-Alday *et al.*, 2004). These authors have inferred a cooling trend following a decline in abundance and diversity before the final inoceramid extinction. The record of the boreal inoceramid *Spyridoceramus tegulatus*, which coincides with the positive $\delta^{18}O$ excursion in their defined stage, E2, throughout the upper part of lithological Unit 5 and Unit 6 , suggests the entry of deep, cold, oxygenated waters arriving from the North Atlantic. These observations confirm the modification of the thermocline and the onset of climatic cooling close to the Early/Late Maastrichtian boundary.

The clear imprint of sea-level fluctuation, as evidenced by the Upper Maastrichtian 3rd-order depositional sequences, with a rhythm of about 1.2 My, is thus consistent with a long-period obliquity influence on sea level. Such type of scenario during the Oligocene has been shown to be related to carbon-cycle events and glacial periodicity. Possible drivers for this long-period linkage between orbital cycles, sea level and the carbon cycle during the Cretaceous greenhouse, a time during which continental ice sheets are presumed to have been either ephemeral or non-existent, have been considered (Wendler *et al.*, 2011). In a study of the Cenomanian-Turonian carbonate platforms in Jordan, these authors postulate that systematic changes in weathering patterns consistent with variable freshwater transport between the ocean and land, support the hypothesis that freshwater storage in aquifers played an important role in modulating eustasy. We believe that the Campanian-Maastrichtian succession in the Basque Basin can in the near future not only contribute towards an improvement of the general chronostratigraphy and a new generation of the Geological Time Scale, but also shed light upon many intriguing palaeoclimatic trends and features in response to orbital forcing.

Conclusions

1) A bed-by-bed comprehensive correlation has been established for the Upper Maastrichtian hemipelagic succession in the Basque Basin at Zumaia, Sopelana I and Hendaia, comprising the classical lithological Units 6–12 described by Wiedmann (1988) which span about 150 m of stratigraphic thickness at Zumaia, equal to ~3.1 My time.
2) An available carbonate proxy record for the uppermost Units 10–12 throughout 64 m of a section containing 72 marl-limestone couplets at Zumaia is used for spectral analysis to recover the full hierarchy of orbital cycles that include, besides the precession-related couplets of 21 ky mean duration, the short (~100 ky) and long (405 ka) eccentricity cycles. Cycle counting and the stacking of eccentricity-related bundles is followed downsection and correlated among the studied sections.
3) Strategic palaeomagnetic sampling was conducted to delineate the two main reversals within the Upper Maastrichtian, the C31r/C31n and

C30n/C29r chron boundaries. The dataset for the upper reddish Units 11–12 at Sopelana I, Zumaia and Hendaia, which should contain C30n/C29r, indicates that those lithologies have been remagnetized by a relatively complex mechanism and appear useless for magnetostratigraphic purposes, casting some doubt on earlier results at Sopelana that we have not been able to reproduce. Instead, the grey lithologies from Unit 6 host a weak but primary magnetization, allowing the unambiguous identification of the C31r/C30n reversal boundary at the three studied sections, which can be placed in a solid cyclostratigraphic template, superseding previous studies.

4) An integrated high-resolution calcareous nannofossil biostratigraphy is established for the entire Upper Maastrichtian, which can now be placed in the cyclo-magnetostratigraphic framework. The succession of the main documented nannofossil bioevents/biohorizons includes: (1) First occurrence (FO) of *Lithraphidites quadratus*; (2) FO of *Micula murus*; (3) FO of *Micula prinsii*. Furthermore, there are two additional bioevents, considered to be of secondary importance, which complement the nannofossil biostratigraphic record. These are the FO of *Cribrosphaerella daniae* and the FRO of *Nephrolithus frequens* in the uppermost part of the section.
5) The solid orbital chronostratigraphic framework indicates that previously established 3rd-order depositional sequences in the Upper Maastrichtian reflect sea-level variations that seem to follow a strong 1.2 My periodicity, reflecting the long obliquity amplitude modulation cycle.
6) The cycle duration estimate relative to the K/Pg boundary for the position of the base of chron C31n, which we propose as an alternative to define the Early/Late Maastrichtian boundary, is 3.08 My (69.08 My with the option of the K/Pg at about 66 My). This is in line with current calibrations of this chron from deep-sea records (Husson *et al*., 2011; Thibault *et al*., 2012).
7) Together with earlier work in the Palaeocene, the extension of the cyclostratigraphic framework into the Maastrichtian, as suggested here, positions the hemipelagic succession in the Basque Basin in a potentially primary role as a geological aid for critical developments of the astronomical solutions that are inaccurate in these older times and also to answer key questions regarding the palaeoclimatic evolution of the Mesozoic greenhouse period in response to orbital forcing.

Acknowledgements

Funding for this research was provided by project CGL2011-23770 of the Spanish Ministerio de Economia y Competividad. JDT acknowledges a sabbatical grant from the Spanish Ministerio de Educación by means of el Programa Nacional de Movilidad de Recursos Humanos del Plan Nacional de I-D+i 2008-2011. Beatriz Bádenas, Lluís Cabrera and an anonymous reviewer are thanked for numerous suggestions that have improved the clarity of the paper. Asier Hilario (Scientific coordinator of the Deba-Zumaia biotope/ Basque Coast Geopark) is thanked for the never failing warmth of his welcome at the Zumaia outcrops.

References

Arz, J.A. and Molina, E. 2002. Bioestratigrafía y Cronoestratigrafía con foraminíferos planctónicos del Campaniense superior y Maastrichtiense de latitudes templadas y subtropicales (España, Francia y Tunicia). *Neues Jahrbuch für Geologie und Paläntologie. Monatshefte,* 224, 161–195.

Baceta, J.I., Pujalte, V., Serra-Kiel, J., Robador, A. and Orue-Etxebarria, X. 2004. El Maastrichtiense final, Paleoceno e Ilerdiense inferior de la Cordillera Pirenaica. In: Vera, J.A., (ed.), *Geología de España*. Sociedad Geológica de España, Instituto Geológico y Minero de España, Madrid, 308–313.

Berger, A. 1978. A simple algorithm to compute long term variations of daily or monthly insolation. Contribution de l'institut d'astronomie et géophysique G. Lemaitre, 18, Université catholique, Louvain-la-Neuve.

Berggren, W.A., Kent, D.V., Swisher C.C. and Aubry M.-P. 1995. A revised Cenozoic geochronology and chronostratigraphy. In: W.A. Berggren, D.V. Kent, M.-P. Aubry, J. Hardenbol (eds.), *Geochronology Time Scales and Global Stratigraphic Correlation* Special. Publication., 54, SEPM, Tulsa, OK, 129–212.

Bown P.R and Young J.R. 1998. Techniques. In: Bown P.R. (ed.) *Calcareous Nannofossil Biostratigraphy*. British Micropalaeontology Society Series. Chapman and Hall/Kluwer Academic Publishers, London, 16–28.

Burnett, J.A., (with contributions from Gallagher, L.T., and Hampton, M.J.), 1998. Upper Cretaceous. In: Bown, P.R. (ed.), *Calcareous Nannofossil Biostratigraphy*. British Micropalaeontological Society Publications Series. Chapman and Hall/Kluwer Academic Publishers, London, 132–199.

Burnett, J.A., Kennedy, W.J. and Ward, P.D. 1992. Maastrichtian nannofossil biostratigraphy in the Biscay region (south–western France, northern Spain). *Newsletters on Stratigraphy*, 26, 145–155.

Dinarès-Turell, J., Baceta, J.I., Pujalte, V., Orue-Etxebarria, X. and Bernaola, G. 2002. Magnetostratigraphic and cyclostratigraphic calibration of a prospective Paleocene/

Eocene stratotype at Zumaia (Basque basin, Northern Spain). *Terra Nova*, 14, 371–378.

Dinarès-Turell, J., Baceta, J.I., Pujalte, V., Orue-Etxebarria, X., Bernaola, G. and Lorito, S. 2003. Untangling the Paleocene climatic rhythm; an astronomically calibrated early Paleocene magnetostratigraphy and biostratigraphy at Zumaia (Basque Basin, northern Spain). *Earth and Planetary Science Letters*, 216, 483–500.

Dinarès-Turell, J., Baceta, J.I., Bernaola, G., Orue-Etxebarria, X. and Pujalte, V. 2007. Closing the Mid-Paleocene gap: toward a complete astronomically tuned Paleocene Epoch and Selandian and Thanetian GSSPs at Zumaia (Basque Basin, W Pyrenees). *Earth and Planetary Science Letters,* 262, 450–467.

Dinarès-Turell, J., Stoykova, K., Baceta, J.I., Ivanov M. and Pujalte, V. 2010. High-resolution intra- and interbasinal correlation of the Danian-Selandian transition (Early Paleocene): the Bjala section (Bulgaria) and the Selandian GSSP at Zumaia (Spain). *Palaeogeography, Palaeoclimatology, Palaeocology*, 297, 511–533.

Dinarès-Turell, J., V. Pujalte, Stoykova, K., Baceta, J.I., and Ivanov M. 2012. The Paleocene "top chron C27n" transient greenhouse episode: evidences from marine pelagic Atlantic and peri-Tethyan sections. *Terra Nova*. doi: 10.1111/j.1365-3121.2012.01086.x

Gardin, S., Galbrun, B., Thibault, N., Coccioni, R., Premoli Silva, I. 2012. Biomagnetochronology for the upper Campanian - Maastrichtian from the Gubbio area, Italy: new results from the Contessa Highway and Bottaccione sections. *Newsletters on Stratigraphy* 45. doi:10.1127/0078-0421/2012/0014.

Gómez-Alday, J.J., López, G. and Elorza, J. 2004. Evidence of climatic cooling at the Early/Late Maastrichtian boundary from inoceramid distribution and isotopes: Sopelana sections, Basque Country, Spain. *Cretaceous Research*, 25, 649–668.

Gómez-Alday, J.J., Zuluaga, M.C., and Elorza, J. 2008. $^{87}Sr/^{86}Sr$ ratios in inoceramids (Bivalvia) and carbonate matrix as indicators of differential diagenesis during burial. Early Maastrichtian Bay of Biscay sections (Spain and France). Potential use for chemostratigraphy?. *Cretaceous Research*, 29, 1–14.

Gradstein, F., Ogg, J. and Smith, A.2004. A Geological Timescale 2004, Cambridge Univ. Press, Cambridge, U. K., doi:10.4095/215638.

Gradstein, F.M., Ogg, J.G., Schmitz, M.D. and Ogg, G.M. 2012. The Geological Time Scale 2012. Elsevier, 1176 pp.

Herbert, T.D. 1999. Towards a composite orbital chronology for the Late Cretaceous and Early Paleogene GPTS. In: Shackleton, N.J., McCave, I.N., Weedon, G.P. (eds.), Philosophical Transactions of the Royal Society of London. A, 1891–1905.

Herbert, T.D., Premoli-Silva, I., Erba, E., Fischer, A.G. 1995. Orbital Chronology of Cretaceous–Paleocene Marine Sediments. In: Berggren, W.A., Kent, D.V., Aubry, M.P., Hardenbol, J. (eds.), Geochronology, Time Scales and Global Stratigraphic Correlation. Spec. Publ., SEPM, 81–93.

Herm, D. 1963. Mikropaläontologisch-stratigraphische untersuchungen im Kreideflisch zwischen Deva und Zumaya (prov. Guipúzcoa, Nordspanien). *Zeitschrift der Deutschen Geologischen Gesellschaft*, 15, 277–348.

Husson, D., Galbrun, B., Laskar, J., Hinnov, L., Thibault, N., Gardin, S. and Locklair, R.E. 2011. Astronomical calibration of the Maastrichtian (late Cretaceous). *Earth and Planetary Science Letters* 305, 328–340.

Hilgen, F. J., Kuiper, K. F. and Lourens L. J. 2010. Evaluation of the astronomical time scale for the Paleocene and earliest Eocene. *Earth and Planetary Science Letters*, 300, 139–151, doi:10.1016/j.epsl.2010.09.044.

Kent, D.V. 1999. Orbital tuning of geomagnetic polarity time-scales. *Phil. Transactions Royal Society London,* 357, 1995-2007.

Kirschvink J.L. 1980. The least-squares line and plane and the analysis of palaeomagnetic data. Geophys. *Geophysical Journal of the Royal Astronomical Society*, 62, 699–718.

Kuiper, K.F., Deino, A., Hilgen, F.J., Krijgsman, W., Renne, P.R. and Wijbrans, J.R. 2008. Synchronizing rock clocks of Earth history. *Science*, 320, 500–504.

Lamolda, M.A. 1985. Biostratigraphie du Maastrichtien basco-cantabrique: ses foraminifères planctoniques. *Géologie Méditerranéenne* 10 (for 1983), 121–126.

Lamolda, M.A. and Gorostidi, A. 1994. Nanoflora y acontecimientos del tránsito Cretácico–Terciario. Una visión desde la región Vascocantábrica. *Revista de la Sociedad Mexicana de Paleontología*, 7, 54–58.

Laskar, J., Robutel, P., Joutel, F., Gastineau, M., Correia, A.C.M. and Levrard, B. 2004. A long-term numerical solution for the insolation quantities of the Earth. *Astron. Astrophys.*, 428, 261–285.

Laskar, J., Gastineau, M., Delisle, J.B., Farrés, A. and Fienga, A. 2011a. Strong chaos induced by close encounters with Ceres and Vesta. *A&A*, 532, L4.

Laskar, J., Fienga, A., Gastineau, M. and Manche, H. 2011b. La2010: A new orbital solution for the long term motion of the Earth. *A&A*, 532, A89.

Lees, J. A. 2007. New and rarely reported calcareous nannofossils from the Late Cretaceous of coastal Tanzania: outcrop samples and Tanzania Drilling Project Sites 5, 9 and 15. *Journal of Nannoplankton Research,* 29, 39-65.

Lees, J.A., Bown, P.R. 2005. Upper Cretaceous calcareous nannofossil biostratigraphy, ODP Leg 198 (Shatsky Rise, northwest Pacific Ocean). Proceedings of the Ocean Drilling Program, Scientific Results 198, 1–60. doi:10.2973/odp.proc.sr.198.114.2005.

Liu, Y., Liang, X.S. and Weisberg, R.H. 2007. Rectification of the bias in the wavelet power spectrum. *Journal of Atmospheric and Oceanic Technology*, 24, 2093–2102.

Lourens, L. J., Hilgen, F. J., Laskar, J., Shackleton, N. J. and Wilson, D. 2004. The Neogene Period. In: F. Gradstein, J. Ogg, and A. Smith (eds.), A Geological Timescale 2004, Cambridge Univ. Press, Cambridge, U. K., 409–440.

MacLeod, K.G. 1994. Extinction of inoceramid bivalves in Maastrichtian strata of the Bay of Biscay region of France and Spain. *Journal of Paleontology*, 68, 1048-1066.

MacLeod, K.G. and Orr, W.N. 1993. The taphonomy of Maastrichtian inoceramids in the Basque Region of France and Spain and the pattern of their decline and disappearance. *Paleobiology*, 19, 235–250.

Mary, C., Moreau, M.G., Orue-Etxebarria, X., Apellaniz, E. and Courtillot, V. 1991. Biostratigraphy and magnetostratigraphy of the Cretaceous/Tertiary Sopelana section (Basque Country). *Earth and Planetary Science Letters,* 106, 133–150.

Mathey, B., 1982. El Cretácico del Arco Vasco. In: García, E. (ed.), *El Cretácico de España*. Universidad Complutense de Madrid, 111–135.

Molina, E., Alegret, L., Arenillas, I., Arz, J.A., Gallala, N., Grajalese Nishimura, M., Murilloe Muñetón, G., Zaghbibe Turki, D. 2009. The Global Boundary Stratotype Section and Point for the base of the Danian Stage (Paleocene, Paleogene, "Tertiary", Cenozoic): auxiliary sections and correlation. *Episodes*, 32, 84–95.

Moreau, M.G., Cojan, I., Ory, J. 1994. Mechanisms of remanent magnetization in marl and limestone alternations. Case study: Upper Cretaceous (Chron 31–30), Sopelana, Basque Country. *Earth and Planetary Science Letters* 123, 15–37

Mount, J.J., Ward, P.D. 1986. Origin of limestone/marl alternations in the Upper Maastrichtian of Zumaya, Spain. *Journal of Sedimentary Petrology*, 56, 228–236.

Paillard, D., Labeyrie, L. and Yiou, P. 1996. Macintosh program performs time-series analysis, *EOS Trans. AGU*, 77, 339.

Paul, C.R.C. and Lamolda, M.A. 2007. Carbon and oxygen stable isotopes in the Maastrichtian of the Basque Country, N. Spain. *Cretaceous Research*, 28, 812–820.

Perch-Nielsen, K. 1985. Mesozoic calcareous nannofossils. In: Bolli, H.M., Saunders, J.B., and Perch-Nielsen, K. (eds.), *Plankton Stratigraphy.* Cambridge Univ. Press, Cambridge, 329–426.

Plaziat, J.C. 1981. Late Cretaceous to Late Eocene palaeogeographic evolution of southwest Europe. *Palaeogeography, Palaeoclimatology, Palaeoecology,* 36, 263–293.

Posamentier, H. W. and Vail, P. R. 1988. Eustatic control on clastic deposition II- Sequence and System Tract models. In: Wilgus C.K. *et al*., (eds.), *Sea-Level Changes: an integrated approach*. SEPM (Society of Economic Paleontologists and Mineralogists) Special Publication, 42, 125–154.

Pujalte, V., Baceta, J.I., Payros, A., Orue-Etxebarria, X. and Serra-Kiel, J. 1994. Late Cretaceous-Middle Eocene Sequence Stratigraphy and Biostratigraphy of the SW. and W. Pyrenees (Pamplona and Basque Basins, Spain), 118 pp., GEP /IGCP 286 Field Seminar Guide-Book, Basque Country Univ., Bilbao.

Pujalte, V., Baceta, J.I., Dinarès-Turell, J., Orue-Etxebarria, X. Parès, J.M. and Payros, A. 1995. Biostratigraphic and magnetostratigraphic intercalibration of late Maastrichtian and Paleocene depositional sequences from the deep-water Basque basin, W Pyrenees, Spain. *Earth and Planetary Science Letters*, 136, 17–30.

Roth, P. H. 1978. Cretaceous nannoplankton biostratigraphy and oceanography of northwestern Atlantic Ocean. *Initial Reports of the DSDP,* 44, 731-760.

Schmitz, B., Pujalte, V., Molina, E., Monechi, S., Orue-Etxebarria, X., Speijer, R.P., Alegret, L., Apellaniz, E., Arenillas, I., Aubry, M-P, Baceta J.I., Berggren, W.A., Bernaola, G., Caballero, F., Clemmensen, A., Dinarès-Turell, J., Dupuis, C., Heilmann-Clausen, C., Hilario Orús, A., Knox, R., Martín-Rubio, M., Ortiz, S., Payros, A., Petrizzo, M.R., Sprong, J., Steurbaut, E. and Thomsen, E. 2011. The global stratotype sections and points for the bases of the Selandian (Middle Paleocene) and Thanetian (Upper Paleocene) stages at Zumaia, Spain. *Episodes*, 34, 220–243.

Sissingh, W. 1977. Biostratigraphy of Cretaceous calcareous nannoplankton. *Geologie en Mijnbouw,* 56, 37-65.

Ten Kate, W.G. and Sprenger, A. 1993. Orbital cyclicities above and below the Cretaceous/Paleogene boundary at Zumaya (N Spain), Agost and Relleu (SE Spain). *Sedimentary Geology*, 87, 69–101.

Thibault, N. 2010. Calcareous nannofossils from the boreal Upper Campanian-Maastrichtian chalk of Denmark. *Journal of Nannoplankton Research,* 31, 1, 39-56.

Thibault, N., Gardin, S., Galbrun, B. 2010. Latitudinal migration of calcareous nannofossil *Micula murus* in the Maastrichtian: Implications for global climate change. *Geology,* 38, 203–206.

Thibault, N., Husson, D., Harlou, R., Gardin, S., Galbrun, B., Huret, E. and Minoletti, F. 2012. Astronomical calibration of upper Campanian-Maastrichtian carbon isotope events and calcareous plankton biostratigraphy in the Indian Ocean (ODP Hole 762C): implication for the age of the Campanian-Maastrichtian boundary. *Palaeogeography, Palaeoclimatology, Palaeoecology,* 337-338, 52-71.

Torrence, C. and Compo, G.P. 1998. A practical guide to wavelet analysis. *Bulletin American Meteorological Society*, 79, 61–78.

von Hillebrandt, A. 1965. Foraminiferen-Stratigraphie im Alttertiär von Zumaia (prov. Guipuzcoa, NW Spanien) und ein Vergleich mit anderen Tethys-Gebieten. Abh. Kön. Bay, Akad. Wiss. München, 123, 1–63.

Varadi, F., Runnegar, B. and Ghil, M. 2003. Successive refinements in long-term integrations of planetary orbits. *Astrophysical Journal*, 592, 620–630.

Ward, P.D., Wiedmann, J. and Mount, J.J. 1986. Maastrichtian molluscan biostratigraphy and extinction patterns in a Cretaceous/Tertiary boundary section exposed at Zumaya, Spain. *Geology*, 14, 899–903.

Ward, P. D. 1988. Maastrichtian ammonite and Inoceramid ranges from the bay of Biscay Cretaceous-Tertiary boundary sections. *Revista Española de Paleontología*, nº Extraordinario, Paleontology and Evolution: Extinction Events, 119–126.

Ward, P.D., Kennedy,W.J., MacLeod, K.G. and Mount, J.F. 1991. Ammonite and inoceramid bivalve extinction patterns in Cretaceous/Tertiary boundary sections of the Biscay region (southwestern France, northern Spain). *Geology* 19, 1181–1184

Ward, P.D. and Kennedy, W.J. 1993. Maastrichtian ammonites from the Biscay Region (France, Spain). *Journal of Paleontology Memoir* , 34, 1–58.

Wendler, J.E., Meyers, S.R., Wendler, I., Vogt, C., Kuss, J. 2011. Drivers of Cyclic Sea Level Change During the Cretaceous Greenhouse: A new Perspective from the Levant Platform (Jordan), Geological Society of America, *Abstracts with Programs*, 43(5), 376.

Westerhold, T., Roehl, U., Raffi, I., Forniaciari, E., Monechi, S., Reale, V., Bowles, J. and Evans, H.F. 2008. Astronomical calibration of the Paleocene time. *Palaeogeography, Palaeoclimatology, Palaeocology*, 257, 377–403.

Westerhold, T., Röhl, U., Donner, B., McCarren, H.K. and Zachos, J.C. 2011. A complete high-resolution Paleocene benthic stable isotope record for the central Pacific (ODP Site 1209). *Paleoceanography*, 26, PA2216, doi:10.1029/2010PA002092.

Westerhold, T., Röhl, U. and Laskar, J. 2012. Time scale controversy: Accurate orbital calibration of the early Paleogene, *Geochemistry Geophysics Geosystems*, 13, Q06015, doi:10.1029/2012GC004096.

Wiedmann, J. 1988. The Basque coastal sections of the K/T boundary –a key to understanding "mass extinctions" in the fossil record. No. Extraordinario. In: Lamolda, M.A., Kauffman, E.G.,Walliser, O.H. (eds.), *Paleontology and Evolution: Extinction Events*. Revista Española de Paleontología, 127–140.

Zijderveld, J.D.A. 1967. AC demagnetisation of rock: analysis of results. In: D.W. Collinson and others (eds.), *Methods in palaeomagnetism*. Elsevier, Amsterdam, 254–286.

Recibido: noviembre 2012
Revisado: diciembre 2012
Aceptado: enero 2013
Publicado: junio 2013